

インドの肺吸虫：スクリアビン肺吸虫および ヒロクチ肺吸虫の形態観察と分子同定

杉山 広¹、アチャリア・ラングシルジ²、シャンティクマール・シン³

¹感染研・寄生動物部、²シーナカリンウイロート大学（タイ）・理学部

³シッキム医科大学（インド）・微生物学部

Morphological observation and molecular identification of *Paragonimus skrjabini* and *P. heterotremus* occurring in India

Hironmu Sugiyama¹, Achariya Rangsiruji² and T. Shantikumar Singh³

¹Department of Parasitology, National Institute of Infectious Diseases

²Department of Biology, Faculty of Science, Srinakharinwirot University

³Department of Microbiology, Sikkim Manipal Institute of Medical Sciences

人獣共通寄生蠕虫症の原因種として重要視されるウェステルマン肺吸虫 *Paragonimus westermani* は、オランダ・アムステルダムの動物園で死亡したベンガルタイガー由来の虫体に対して、今から約130年前に最初に命名された (Kerbert, 1878)。インドでは、それ以前に *P. compactus* が記載され (Cobbolt, 1859)、その後には *P. edwardsi* が報告された (Gulati, 1926) が、もっぱらウェステルマン肺吸虫が人獣に寄生し、病害を与えていると考えられてきた (Rao, 1935; Srivastava, 1938; Singh *et al.*, 1986)。これは成虫を得て形態から種名を確定すると云う基本的な作業が、インドでは最近までなおざりにされてきたからで、この為にインド各地に分布する肺吸虫の種 (分類・同定) に関しては、未だに不確かな点が数多く残されている。

今回、インド東北部のマニプル州に分布する2種類の肺吸虫について、形態学的特徴を再検討し、また塩基配列を解読して分子同定と系統関係の解析を行う機会を得た。その検索の結果、これらはウェステルマン肺吸虫ではなく、スクリアビン肺吸虫 *P. skrjabini* とヒロクチ肺吸虫 *P. heterotremus* である事が確認された。

スクリアビン肺吸虫は中国全土に広く分布し、人ではしばしば皮下寄生する事が知られている。タイやネパール

にも分布が示唆されているが、インドでは我々の報告が最初の記録となる。また、本邦固有の種とされる宮崎肺吸虫 *P. miyazakii* が本虫の亜種であるとの見解も提出されており (Blair *et al.*, 2005)、インド産のスクリアビン肺吸虫がこれら肺吸虫類の分類学的問題を考える上で、重要な役割を果たす事も期待される。一方でヒロクチ肺吸虫は、中国南部から東南アジアを経てインド北東部 (アルナチャール・プラディッシュ州) にまで分布し、特にタイでは分布する6種の肺吸虫のうち、唯一の人体寄生種として重視されている。インドでも人体寄生種として、公衆衛生上極めて重要な役割を演じているものと想定される。今後も更に検討を進め、今回確認した2種類の肺吸虫が、インドではどのような生活環を営み、人獣に対して具体的にどのような病害を与えているのか、明かにしていく予定である。

Key Words : *Paragonimus skrjabini*, *Paragonimus heterotremus*, India

連絡責任者：杉山 広, 国立感染症研究所寄生動物部,
162-8640東京都新宿区戸山1-23-1, E-mail:hsugi@nih.go.jp

Correspondence: H. SUGIYAMA, Department of
Parasitology, National Institute of Infectious Diseases,
Toyama 1-23-1, Shinjuku-ku, Tokyo 162-8640

Participation of both Host and Virus Factors in Induction of Severe Acute Respiratory Syndrome (SARS) in F344 Rats Infected with SARS Coronavirus[∇]

Noriyo Nagata,^{1*} Naoko Iwata,¹ Hideki Hasegawa,¹ Shuetsu Fukushi,² Masaru Yokoyama,³ Ayako Harashima,¹ Yuko Sato,¹ Masayuki Saijo,² Shigeru Morikawa,² and Tetsutaro Sata¹

Departments of Pathology¹ and Virology 1,² and Center for Pathogen Genomics,³ National Institute of Infectious Diseases, Tokyo, Japan

Received 9 September 2006/Accepted 20 November 2006

To understand the pathogenesis and develop an animal model of severe acute respiratory syndrome (SARS)-associated coronavirus (SARS-CoV), the Frankfurt 1 SARS-CoV isolate was passaged serially in young F344 rats. Young rats were susceptible to SARS-CoV but cleared the virus rapidly within 3 to 5 days of intranasal inoculation. After 10 serial passages, replication and virulence of SARS-CoV were increased in the respiratory tract of young rats without clinical signs. By contrast, adult rats infected with the passaged virus showed respiratory symptoms and severe pathological lesions in the lung. Levels of inflammatory cytokines in sera and lung tissues were significantly higher in adult F344 rats than in young rats. During *in vivo* passage of SARS-CoV, a single amino acid substitution was introduced within the binding domain of the viral spike protein recognizing angiotensin-converting enzyme 2 (ACE2), which is known as a SARS-CoV receptor. The rat-passaged virus more efficiently infected CHO cells expressing rat ACE2 than did the original isolate. These results strongly indicate that host and virus factors such as advanced age and virus adaptation are critical for the development of SARS in rats.

The epidemic of severe acute respiratory syndrome (SARS) spread rapidly worldwide during the winter of 2003 to 2004 (16; <http://www.who.int/csr/sars/country/en/>). SARS-associated coronavirus (SARS-CoV) has been identified as the etiological agent of SARS (4, 5, 12, 14, 28). SARS-CoV has caused progressive respiratory failure and death of approximately 800 individuals, approximately 10% of over 8,000 patients (<http://www.who.int/csr/sars/country/en/>). Common symptoms of SARS are fever, nonproductive cough, myalgia, and dyspnea. An age of 60 years or older, comorbid disease, male sex, high neutrophil counts, and several biochemical abnormalities are associated with poor outcomes (1, 3, 16, 27, 38). Advanced age in particular is recognized as an independent correlate of adverse outcomes and a predictor of mortality.

Experimental animals, particularly monkeys, have been infected with SARS-CoV to analyze various pathogenic aspects of SARS according to Koch's postulates and to develop animal models to evaluate potential vaccines and antiviral agents (2, 5, 6, 7, 14, 17, 24, 30, 31, 34). Cats, ferrets, mice, pigs, guinea pigs, hamsters, chickens, and rats have also been investigated for SARS-CoV susceptibility (22, 23, 32, 33, 39). All these animals are susceptible to SARS-CoV after intraspiratory inoculation and exhibit virus excretion in pharyngeal or nasal swabs, histopathological pulmonary lesions, and seroconversion. In monkeys, aged mice, and Syrian hamsters, infection is not lethal but results in consolidative pneumonitis that resolves within 1 week (7, 24, 30, 32, 33, 34). Thus, existing animal

models are useful to analyze the pathology associated with early phases of SARS-CoV infection and to provide insights into early events in SARS-CoV infection.

The SARS-CoV spike (S) protein mediates the infection of receptor-bearing cells. In the case of several avian and mammalian coronaviruses, the S protein is cleaved by furin or a related protease into S1 and S2 proteins. The S1 protein bears the receptor attachment site, and the S2 protein mediates fusion activity (15). Angiotensin-converting enzyme 2 (ACE2) is a functional receptor for SARS-CoV that binds SARS-CoV S protein with a high affinity (18, 19, 20). Several reports suggest that ACE2 is a physiologically relevant receptor during infection. Its protein expression pattern corresponds to the localization of virus infection in humans and animals (10, 35). Also, the efficiency of infection in humans and other species correlates with the ability of ACE2 in that species to support viral replication (18, 21). Structural analysis of the peptidase domain of human, palm civet, mouse, and rat ACE2 with the SARS-CoV receptor-binding domain of S1 has identified aspects of that interface that enable efficient cross-species infection and human-to-human transmission (18). Interestingly, rat ACE2 does not support infection by SARS-CoV.

The objectives of this study were to understand the pathogenesis of and develop an animal model for SARS. We found that the Frankfurt 1 isolate of SARS-CoV replicated in the respiratory tracts of F344 rats without associated clinical symptoms. We passaged the Frankfurt 1 isolate serially in young F344 rats and found that by the 10th passage, the virus was altered such that it replicated more efficiently in rats than did the original virus. Furthermore, adult rats showed more severe acute lung injury than did young rats after infection with the passaged virus. Higher levels of cytokines were seen in adult

* Corresponding author. Mailing address: Department of Pathology, National Institute of Infectious Diseases, Gakuen 4-7-1, Musashimurayama, Tokyo 208-0011, Japan. Phone: 81-42-561-0771. Fax: 81-42-561-6572. E-mail: nnagata@nih.go.jp.

[∇] Published ahead of print on 6 December 2006.

rats than in young rats after infection. Analysis of the nucleotide sequence of passaged virus encoding relevant S1 domains identified a missense mutation in the receptor binding domain. We found that this mutation is responsible for more efficient viral replication in rats. Comparative analysis of immune responses including an elevation in cytokine levels and histopathological findings in young and adult animals is crucial for understanding SARS pathogenesis.

MATERIALS AND METHODS

Viruses and cells. The SARS-CoV Frankfurt 1 isolate used here was kindly supplied by John Ziebuhr, Institute of Virology and Immunology, University of Würzburg, Würzburg, Germany. Virus was propagated twice in Vero E6 cells purchased from the American Type Culture Collection (Manassas, VA). Vero E6 cells were cultured in Eagle's minimal essential medium (MEM) containing 5% fetal bovine serum, 50 IU of penicillin G, and 50 µg of streptomycin per ml. Titers of this stock were expressed as 50% of the tissue culture infectious dose (TCID₅₀), which was calculated according to the Behrens-Kärber method using Vero E6 cells. Work with infectious SARS-CoV was performed under biosafety level 3 conditions.

Experimental infection of rats with SARS-CoV. F344 rats (4-week-old females purchased from Japan SLC, Inc.) were inoculated intranasally with SARS-CoV in a volume of 100 µl into the left nostril under anesthesia using an intraperitoneal injection of 0.1 ml/10 g body weight of 1.00 mg of ketamine (Ketalar) plus 0.02 mg of xylazine. Each animal was bled under ether anesthesia and sacrificed on days 3, 5, 7, and 21 postinoculation (p.i.). Animals were housed in biosafety level 3 animal facilities. Protocols for animal experiments were approved by the Animal Care and Use Committee of the National Institute of Infectious Diseases, Tokyo, Japan.

Serial in vivo passage of SARS-CoV in rats. The Frankfurt 1 isolate was serially passaged 10 times in 4-week-old female F344 rats. After intranasal inoculation, three rats were sacrificed on day 3 p.i. to collect bronchoalveolar wash fluids. Lungs were removed under sterile conditions, washed three times, and homogenized in 2 ml phosphate buffer containing 0.1% bovine serum albumin, 20 IU of penicillin G, 20 µl of streptomycin, and 1 µg of amphotericin B per ml. The wash fluid was then serially inoculated into F344 rats 10 times. At the 5th and 10th passage, wash fluids (F-ratV and F-ratX, respectively) were checked for virulence in rats. After 10 passages, lung homogenates were centrifuged at 2,000 rpm for 20 min, and the supernatant was used to infect Vero E6 cells. Cells were infected with 1 ml of the homogenates in 10 ml of MEM containing 2% fetal bovine serum. After 1 h of absorption, the inoculum was removed, and MEM containing 2% fetal bovine serum was added. Infected cell cultures were continuously incubated at 37°C with 5% CO₂. Cells were harvested 2 days after infection and treated once by freeze-thawing. After centrifugation at 2,000 rpm for 20 min, the supernatant was used as the virus inoculum (F-ratX-VeroE6).

Frankfurt 1, F-ratV, F-ratX, and F-ratX-VeroE6 were intranasally inoculated into 4-week-old female F344 rats. While still under ether anesthesia, the rats were bled and sacrificed by exsanguination on days 3, 5, 7, and 21 p.i., respectively. Three of the six rats were analyzed for virus replication and cytokine responses, and the other three were investigated histopathologically on each day. F-ratX-VeroE6 was similarly inoculated into adult F344 rats (7- to 8-month-old males purchased from Charles River, Inc., Japan). After intranasal inoculation with 100 µl of the virus, three adult rats were bled under ether anesthesia and killed by exsanguination on days 3, 5, and 7 p.i. to analyze virus replication and cytokine responses. Adult rats were also used for pathological examination on days 3, 5, 7, 14, and 21 p.i. Follow-up experiments were performed using 200 µl of strain F-ratX-VeroE6 using adult rats for pathological examination on days 3, 5, 7, and 14 p.i.

Virus isolation and titration. Tissue homogenates (20% [wt/vol]) from lung or maxilla including nasal cavity were prepared in MEM containing 2% fetal bovine serum, 50 IU of penicillin G, 50 µg of streptomycin, and 2.5 µg of amphotericin B per ml. Samples were clarified by centrifugation at 2,000 rpm for 20 min, and supernatants were inoculated onto VeroE6 cell cultures for virus isolation and titration.

Neutralizing antibody. Plasma samples were diluted twofold in a range from 1:10 to 1:320 with MEM containing 2% fetal bovine serum, 50 IU of penicillin G, 50 µg of streptomycin, and 2.5 µg of amphotericin B per ml. Each sample was mixed with the same volume of MEM containing SARS-CoV at an infectious dose of 100 TCID₅₀ per 100 µl, and the mixture was incubated for 1 h at 37°C for neutralization. After incubation, 100 µl of each sample was inoculated onto

monolayers of Vero E6 cells in 96-well culture plates, which were incubated at 37°C with 5% CO₂. After 48 h, cells were examined for cytopathic effects (CPEs). The neutralizing antibody was determined as a reciprocal of the highest dilution at which a CPE was not observed.

Histopathology and immunohistochemistry. Animals were anesthetized and perfused with 10 ml of 10% phosphate-buffered formalin. Fixed tissues of lung, heart, kidney, liver, spleen, small and large intestine, brain, spinal cord, and maxilla including nasal cavity were routinely embedded in paraffin, sectioned, and stained with hematoxylin and eosin. Maxilla samples were decalcified in phosphate-buffered saline (PBS) (pH 7.4) plus 10% EDTA before embedding. Immunohistochemical detection of the SARS-CoV and ACE2 antigens was performed on paraffin-embedded sections. Rabbit antibodies against SARS-CoV and recombinant human ACE2 (R&D Systems, MN) were used as first antibodies. After deparaffinizing with xylene, sections were hydrated in ethanol and immersed in PBS. Antigens were retrieved by hydrolytic autoclaving for 20 min at 121°C in 10 mM/liter sodium citrate-sodium chloride buffer (pH 6.0). After cooling, sections were immersed in PBS. Endogenous peroxidase was blocked by 1% hydrogen peroxide in methanol for 30 min. After washing in PBS, the sections were treated with normal rabbit serum for 5 min and then incubated with antibodies against SARS-CoV or ACE2 overnight at 4°C. After three washes in PBS, the sections were incubated with biotin-conjugated anti-rabbit immunoglobulin G for 30 min at 37°C, followed by streptavidin-peroxidase for 30 min at room temperature. Peroxidase activity was developed in diaminobenzidine with hydrogen peroxide. Nuclei were counterstained by hematoxylin.

RNA extraction, RT-PCR, and sequencing. One hundred microliters of wash fluids and lung homogenates was treated with TRIzol (Invitrogen, Gaithersburg, MD) according to the manufacturer's instructions and then treated with DNase I (Promega, Madison, WI). RNA was dissolved in 20 µl RNase-free water. RNA extracted from the wash fluids and lung homogenates was used to generate cDNA. One microgram of eluted RNA samples was reverse transcribed using the Improm-II reverse transcription (RT) system (Promega, Madison, WI) in a 20-µl reaction mixture containing 0.5 µg of random primers, 0.5 mM of deoxynucleoside triphosphates, 30 units of rRNasin RNase inhibitor, and 4 mM of MgCl₂. Mixtures were annealed at 25°C for 5 min and then incubated at 42°C for 60 min for extension, followed by heat inactivation at 70°C for 15 min. Reverse-transcribed products were stored at -20°C. A primer pair targeting the ORF7b region of SARS-CoV sequences (27415P [5'-CTCTTGCTGACAAATAAT-3'] and 27790N [5'-GAGAAGTTTCATGTTTCGT-3']) was used to detect deletion mutants. For PCR, 2.0 µl of cDNA was amplified in a 50-µl reaction mixture containing 0.2 µM each of forward and reverse primers and a high-fidelity PCR Master kit (Roche Diagnostics, Indianapolis, IN). PCR was performed as follows: (i) 4 min at 94°C and then (ii) 35 cycles, with 1 cycle consisting of 1 min at 94°C, 90 s at 55°C, and 2 min at 72°C. Products were analyzed by agarose gel electrophoresis. Water controls were included in each assay, and no false positives were observed in negative-control reactions.

In subsequent experiments, four pairs of primers targeted to spike coding region sequences (nucleotides 20751 to 26610) were used to analyze the virus genome from lung homogenates. Regions and primers were as follows: PCR15-2 (5'-AATACACCTACTTTAGCTGTACCCTACAAC-3') and Sr10 (5'-ATCAC CGACTGTGACTTG-3') for region 1, Seq51 (5'-TTGTCCGTGGTGGGTT TTTGG-3') and PCR16R (5'-GTAATAAAGAACTGTATGGTAACACTAGC AC-3') for region 2, PCR17 (5'-CAGCTTGGCGCATATATCTACTGAAAA C-3') and Sr4 (5'-CCATTGAACTTCTGCGCA-3') for region 3, and Sr7 (5'-C CTGACCCCTCTAAAGCCA-3') and PCR18R (5'-TCTGTAGACAACAGCAA GCACAAAACAAGC-3') for region 4. For PCR, 1.0 µl of cDNA was amplified in a 50-µl reaction mixture containing 0.15 µM each of forward and reverse primers using the Expand Long PCR system (Roche Diagnostics, Indianapolis, IN). PCR was performed as follows: (i) 2 min at 94°C and (ii) 40 cycles, with 1 cycle consisting of 10 s at 94°C, 30 s at 55°C, and 8 min at 68°C. Correctly sized products were purified by using a QIAquick gel extraction kit (QIAGEN GmbH, Germany) and sequenced using a BigDye Terminator v3.1 Cycle Sequencing kit (Applied Biosystems, Foster City, CA). Sequencing products were analyzed by using an ABI PRISM 3700 DNA analyzer (Applied Biosystems, Foster City, CA). Both sense and antisense sequences of PCR products were sequenced at least once.

Cytokine multiplex analysis. Samples of sera and supernatants of 20% homogenates of lungs were analyzed for 10 cytokines (interleukin-1α [IL-1α], IL-1β, IL-2, IL-4, IL-6, IL-10, IL-12, tumor necrosis factor alpha [TNF-α], gamma interferon [IFN-γ], and granulocyte-macrophage colony-stimulating factor) with Luminex 200 (Luminex Co. Austin, TX) using a Rat Cytokine 10-plex antibody bead kit (BioSource International, Inc., Camarillo, CA) according to the manufacturer's instructions. Both samples were subjected to UV irradiation for 10 min and stored at -80°C. Homogenized lung tissue samples were diluted

1:1 in cell extraction buffer (10 mM Tris, pH 7.4, 100 mM NaCl, 1 mM EDTA, 1 mM EGTA, 1 mM NaF, 20 mM $\text{Na}_2\text{P}_2\text{O}_7$, 2 mM Na_3VO_4 , 1% Triton X-100, 10% glycerol, 0.1% sodium dodecyl sulfate, and 0.5% deoxycholate; BioSource International, Inc., Camarillo, CA) for 30 min on ice with vortexing at 10-min intervals and centrifuged at 13,000 rpm for 10 min at 4°C. Supernatants were diluted 1:5 in assay diluent and assayed. Multiplex beads were vortexed and sonicated for 30 s, and 25 μl was added to each well of a 96-well filter plate and washed twice with wash buffer. Samples were diluted 1:2 with assay diluent and loaded onto a Millipore Multiscreen BV 96-well filter plate to which 50 μl of incubation buffer had been added to each well. Serial dilutions of cytokine standards were prepared in parallel and added to the plate. Samples were incubated on a plate shaker in the dark at room temperature for 2 h. The plate was applied to a Millipore Multiscreen vacuum manifold and washed twice with 200 μl wash buffer, and 100 μl of biotinylated anti-rat multicytokine detector antibody was added to each well. The plate was shaken again as described above for 1 h, applied to a Millipore Multiscreen vacuum manifold, and washed twice with 200 μl wash buffer. One hundred microliters of streptavidin R-phycoerythrin was added directly to each well, and the plate was shaken again as described above for 30 min, applied to the vacuum manifold, and washed twice. One hundred microliters of wash buffer was added to each well, and the plate was shaken for 3 min. The assay plate was analyzed using the Bio-Plex Luminex 100 XYP instrument. Cytokine concentrations were calculated using Bio-Plex Manager 3.0 software with a five-parameter curve-fitting algorithm applied for standard curve calculations.

Infection of rat ACE2-expressing CHO cells with in vivo-passaged SARS-CoV. Rat ACE2 cDNA was amplified by PCR from reverse-transcribed rat kidney RNA using primers mACE2f2 (5'-TTGCTCAGTGGATGGGATCTTGGC-3') and ratACE2r1 (5'-GCATACAGTAAAATGACGACGAGTG-3') and cloned into a pcDNA 3.1(+) vector (Invitrogen, Grand Island, NY). A variant rat ACE2 gene with amino acid residues 82 to 84 (NYS) altered to residues corresponding to human ACE2 (MYP) was generated as described previously by Li et al. (20) and cloned into pcDNA 3.1(+). CHO cells were transfected with plasmids encoding either form. Cells were infected with the Frankfurt 1 isolate or F-ratX-VeroE6 at a multiplicity of infection of 0.002, and culture supernatants were harvested 72 h p.i. for virus titration.

Molecular modeling of a complex of rat-passaged SARS-CoV spike protein and rat ACE2. To predict the three-dimensional (3-D) structure of the receptor binding domain of rat-passaged SARS-CoV spike protein complexed with rat ACE2, we used the crystal structure of the receptor binding domain of SARS-CoV spike protein/human ACE2 complex at a 2.9-Å resolution (Protein Data Bank accession number 2AJF) (18) as a template for homology modeling. 3-D models were constructed independently by a homology modeling technique using MOE-Align and MOE-Homology in the Molecular Operating Environment (MOE) (Chemical Computing Group Inc., Canada) as described previously (11). 3-D structures were thermodynamically optimized by energy minimization using MOE and an AMBER99 force field (29). Physically unacceptable local structures of optimized 3-D models were further refined using the Ramachandran plot program packaged in MOE.

Statistical analysis. All data were analyzed by Student's *t* test.

RESULTS

Enhanced virulence of SARS-CoV after serial in vivo passage in rats. Three days after intranasal inoculation with the Frankfurt 1 isolate of SARS-CoV, histopathological lesions in lungs of young F344 rats (4-week-old females, three rats per group) were mild, and virus antigen-positive cells were rarely seen (Fig. 1A). During 10 serial passages of the Frankfurt 1 isolate, the virus was consistently identified in the maxillary tissue, including the nasal cavity, lung tissue, and lung fluids (Fig. 1B). In nasal wash fluids, infectious virus was not detectable after the fourth passage.

It has been reported that a variant of the Frankfurt 1 isolate emerged in which 45 nucleotides (nucleotides 27670 to 27714) are deleted within ORF7b upon replication in cell culture (36). Thus, the Frankfurt 1 isolate used in the present study was a mixture of the original virus without the deletion and a variant carrying the deletion (Fig. 1C). A variant with the deletion in the ORF7b region was detected in nasal and lung washes of

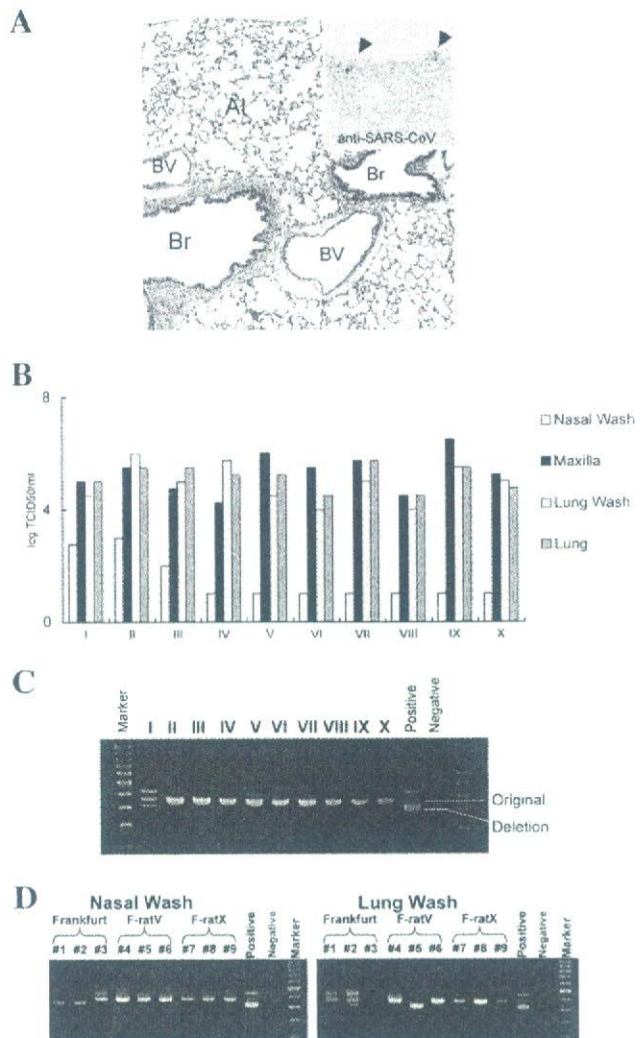


FIG. 1. Experimental infection and serial in vivo passages of SARS-CoV in young F344 rats (4-week-old females; $n = 3$). (A) Hematoxylin- and eosin-stained tissue section of lung. After intranasal inoculation with the Frankfurt 1 isolate, no inflammatory reaction in bronchi was observed. A few virus-positive cells in bronchi were seen by immunohistochemistry using SARS-CoV-specific antibody (inset, arrowheads). Br, bronchi; Al, alveoli; BV, blood vessel (magnification, $\times 20$; inset magnification, $\times 40$). (B) Virus titers were detected in the maxilla including nasal cavity and lung tissue homogenates and lung wash fluids following 10 serial passages. The detection limit was $10^{1.5}$ TCID₅₀/g of tissue. (C) DNA of serially passaged virus was amplified by RT-PCR of lung wash fluids using primers specific for ORF7b-encoding cDNA. No ORF7b deletion mutant was replicated during the serial passage. Positive indicates that the Frankfurt 1 isolate was amplified by RT-PCR; negative indicates that distilled water was used as a negative control. (D) Viral DNA was amplified by RT-PCR of nasal and lung wash fluids on day 3 p.i. using ORF7b primers. A 45-nucleotide in-frame deletion in ORF7b was detected in nasal and lung wash fluid from one animal (animal 3) and two animals (animals 1 and 2) after infection with the Frankfurt 1 isolate, respectively. F-ratV and F-ratX virus were passaged 5 and 10 times serially, respectively. The same positive and negative controls were used in C.

Frankfurt 1-infected rats; however, during serial passage in vivo, that variant was not detected (Fig. 1C and D). Replication and pathogenicity of the 5th and 10th serially passaged viruses (referred to as F-ratV and F-ratX, respectively) in the

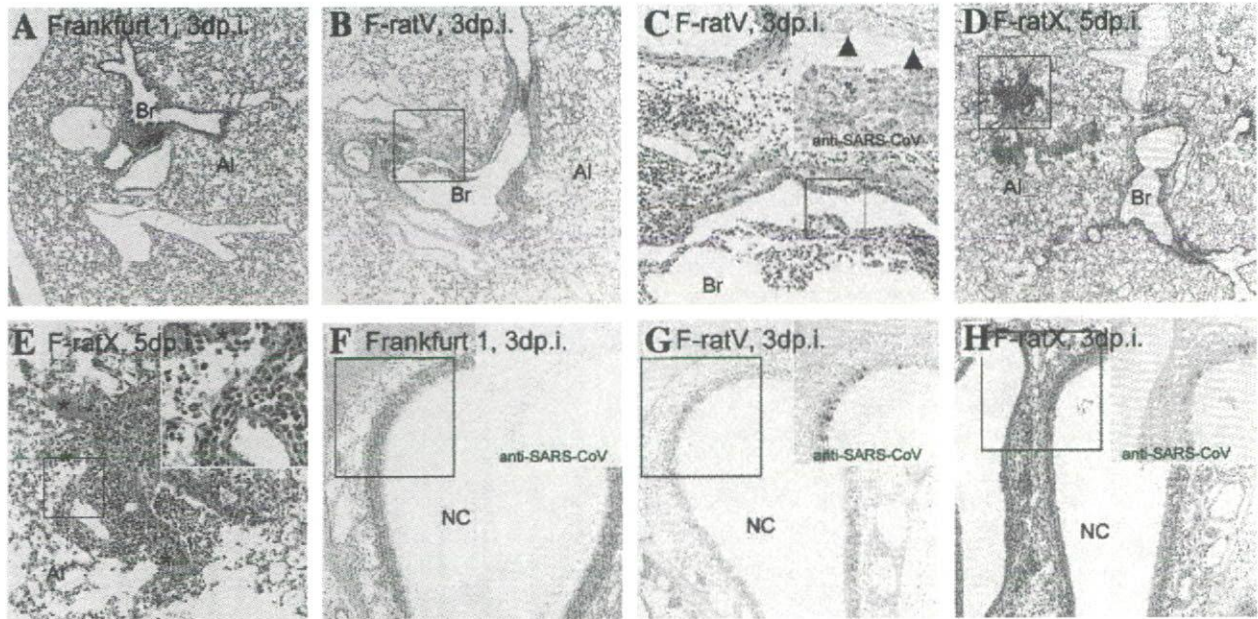


FIG. 2. Histopathologies of lung (A to E) and nasal cavity (F to H) in young F344 rats (4-week-old females; $n = 3$) after intranasal inoculation with serially passaged virus. Br, bronchi; Al, alveoli; NC, nasal cavity. (A) No inflammatory infiltrates in lung after inoculation with the Frankfurt 1 isolate were observed on day 3 p.i. (hematoxylin and eosin staining) (magnification, $\times 10$). (B and C) Slight inflammatory reactions around bronchioles were observed in F344 rats after intranasal inoculation with five-times-serially-passaged Frankfurt 1 strain F-ratV on day 3 p.i. (C) Extensive cellular debris in bronchioles comprised of necrotic epithelia and inflammatory cells (magnification, $\times 50$). Immunohistochemical staining using SARS-CoV-specific antibody detected virus antigen-positive cells in bronchioles and epithelial cells (C, inset) (immunohistochemistry) (magnification, $\times 100$). (D and E) Expanded inflammatory reactions around bronchioles and the alveolar area were observed in F344 rats after inoculation with 10-times-serially-passaged Frankfurt 1 strain F-ratX on day 5 (magnifications, $\times 10$ [D], $\times 50$ [E], and $\times 100$ [inset]) p.i. Small hemorrhages (*) and infiltration of lymphocytes were observed in peribronchiolar alveoli (E, inset). (F) No inflammatory reactions or virus antigen-positive cells were observed in the nasal cavity after inoculation with the Frankfurt 1 isolate on day 3 p.i. (G) Degenerated virus antigen-positive epithelial cells were observed in the nasal cavity after inoculation with F-ratV on day 3 p.i. (H) Massive inflammatory reactions and virus antigen-positive cells were observed in the nasal cavity after inoculation with F-ratX on day 3 p.i. (magnification, $\times 25$ [F to H]).

respiratory tract of young F344 rats were higher than that seen with the original Frankfurt 1 isolate (Fig. 2 and Table 1). Young F344 rats inoculated with the original Frankfurt 1 isolate showed neither inflammatory lesions in lung nor virus antigen-positive cells in the nasal cavity on day 3 p.i. (Fig. 2A and F). After intranasal inoculation with F-ratV, virus antigens were observed immunohistochemically in the respiratory epithelia of the trachea, bronchi, and nasal cavity, which was accompanied by slight inflammatory reactions on day 3 p.i. (Fig. 2B, C, and G). More virus antigen-positive cells were seen in respiratory epithelia including the alveolar area of strain F-ratX-inoculated rats than in Frankfurt 1- or F-ratV-inoculated rats along with severe inflammatory reactions (Fig. 2D,

E, and H). Inflammatory reactions, including neutrophils, macrophages, and lymphocytes, as well as microhemorrhage, were seen on day 5 p.i. (Fig. 2D and E). Thus, serial in vivo passage of virus in young rats increased SARS-CoV virulence. None of young F344 rats inoculated with the Frankfurt 1 isolate, F-ratV, or F-ratX showed any obvious clinical signs, and they survived until the observation period.

Increased pathogenicity of serially passaged SARS-CoV in adult rats. In humans, advanced age is associated with greater mortality in SARS patients. Thus, we analyzed potential differences in clinical and pathological features following infection of young (4-week-old females) and adult (7- to 8-month-old males) rats with F-ratX. Since quantities of the F-ratX

TABLE 1. Experimental infection with SARS-CoV in F344 rats

Animal age	Virus strain (100- μ l inoculum)	No. of animals with inflammatory reaction/total no. of animals (no. of virus-positive animals/total no. of animals) ^a						No. of neutralization antibody-positive animals/total no. of animals (titers of antibody to Frankfurt)
		3 days p.i.		7 day p.i.		21 days p.i.		
		Nasal cavity	Lung	Nasal cavity	Lung	Nasal cavity	Lung	
4 wk	Frankfurt	0/3 (1/3)	0/3 (0/3)	0/3 (0/3)	0/3 (0/3)	0/3 (0/3)	0/3 (0/3)	3/3 (2 ⁶ , 2 ⁷ , 2 ⁷)
4 wk	F-ratX-VeroE6	3/3 (3/3)	3/3 (3/3)	3/3 (3/3)	3/3 (3/3)	0/5 (0/5)	4/5 (0/5)	5/5 (2 ⁷ , 2 ⁷ , 2 ⁷ , 2 ⁸ , <2 ⁸)
7-8 mo	F-ratX-VeroE6	3/3 (3/3)	3/3 (3/3)	NE	3/3 (2/3)	NE	2/2 (0/2)	2/2 ^b (2 ⁷ , <2 ⁸)

^a NE, not examined.

^b Sera were collected on day 14 p.i.

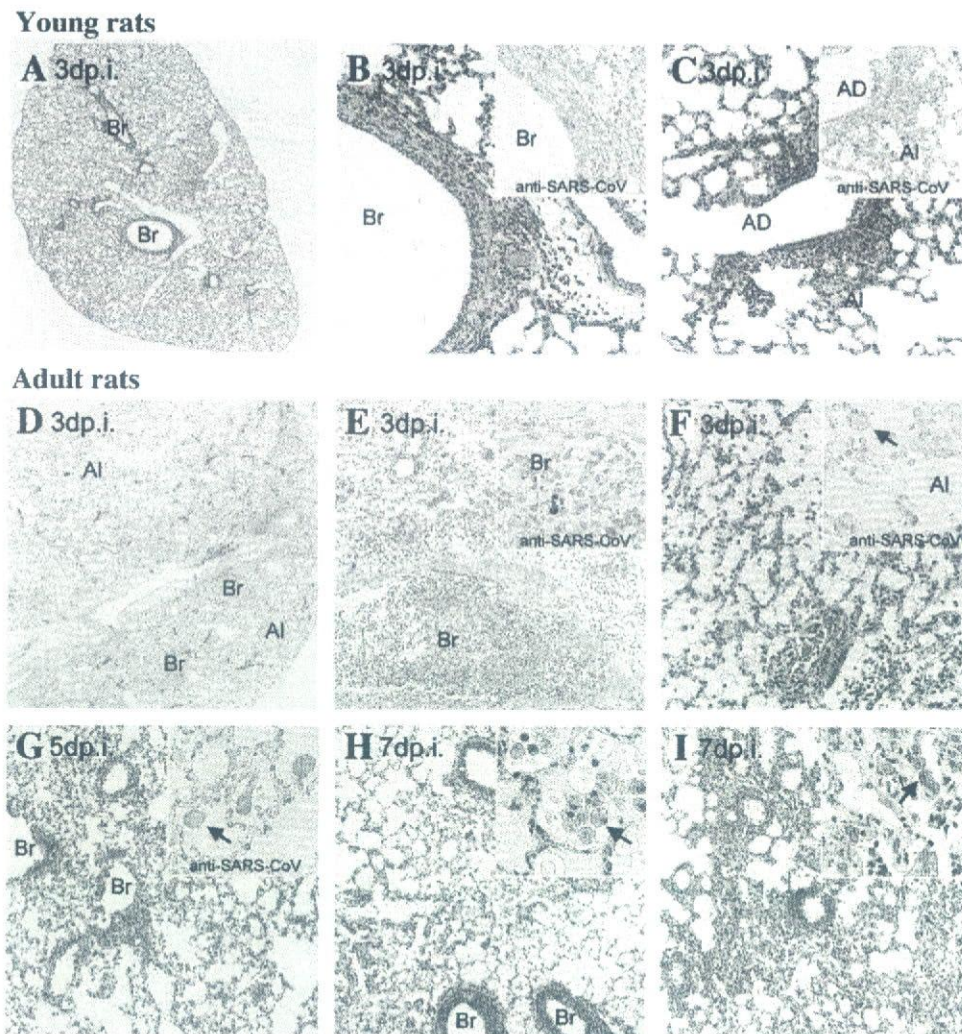


FIG. 3. Histopathological findings in lungs of young and adult F344 rats after intranasal infection with 10-times-serially-passaged SARS-CoV strain F-ratX-VeroE6 on days 3, 5, and 7 p.i. ($n = 3$). Br, bronchi; Al, alveoli; AD, alveolar duct. (A to C) Inflammatory reactions were observed around the bronchi with leukocytes and lymphocytes (B) and alveolar ducts and alveoli (C) of young F344 rats on day 3 p.i. Immunohistochemical staining with SARS-CoV-specific antibody detected virus antigen-positive cells in those epithelial cells (B and C, insets). (D to F) Massive inflammatory reactions with pulmonary edema and neutrophil and activated macrophage infiltrations were observed in lungs of adult F344 rats on day 3 p.i. Bronchi and alveoli were filled with extensive cellular debris comprised of necrotic epithelia and inflammatory cells (E and F). Immunohistochemical staining by SARS-CoV-specific antibody detected virus antigen-positive cells in necrotic cells and alveolar macrophages (arrow) (E and F, insets). (G) SARS-CoV antigen-positive cells in the alveolar macrophages of adult F344 rats on day 5 p.i. (H and I) Various stages of the inflammatory response and regeneration reaction in the alveoli of adult F344 rats on day 7 p.i. Necrotic macrophages (H, arrow) and effusion substances in alveoli (H, inset) are shown. Mononuclear cell infiltrations and regenerated type II alveolar cells (I, arrow) in alveoli (I, inset) are shown. Magnifications, $\times 5$ (A and D), $\times 25$ (E and G to I), $\times 50$ (B, C, and F), and $\times 100$ (E to I, insets).

preparation were limited, the virus was propagated once in Vero E6 cells (referred to as F-rat-X-VeroE6) before inoculation.

Histopathological features of the lung tissue 3 days after infection with the F-ratX-VeroE6 strain ($100 \mu\text{l}$ of $10^{6.4}$ TCID₅₀) differed between young and adult rats (Fig. 3 and Table 1). In young rats without clinical symptoms, inflammatory infiltrates were seen around bronchi, bronchioles, and alveoli (Fig. 3A to C). Virus antigen-positive cells were located at epithelia of the bronchi, bronchioles, and alveoli at day 3 p.i. (Fig. 3B and C, inset). Inflammatory cells such as neutrophils, macrophages, and lymphocytes infiltrated around the affected

respiratory tracts (Fig. 3B and C). Mild edema was seen around blood vessels (Fig. 3B). By contrast, after infection, adult rats became lethargic and showed ruffled fur and abdominal breathing. Grossly, a few lobes of the lungs showed congestion, edema, and consolidation at days 3 and 5 p.i. Furthermore, the inflammatory reaction, especially pulmonary edema, was more severe in adult than in young rats (Fig. 3D). Histopathological features of lung tissue on days 3 (Fig. 3E and F), 5 (Fig. 3G), and 7 (Fig. 3H and I) p.i. showed bronchiolitis obliterans organizing pneumonia and diffuse alveolar damage, which are observed in early phases of human SARS. The major inflammatory cells in alveoli were neutrophils and activated

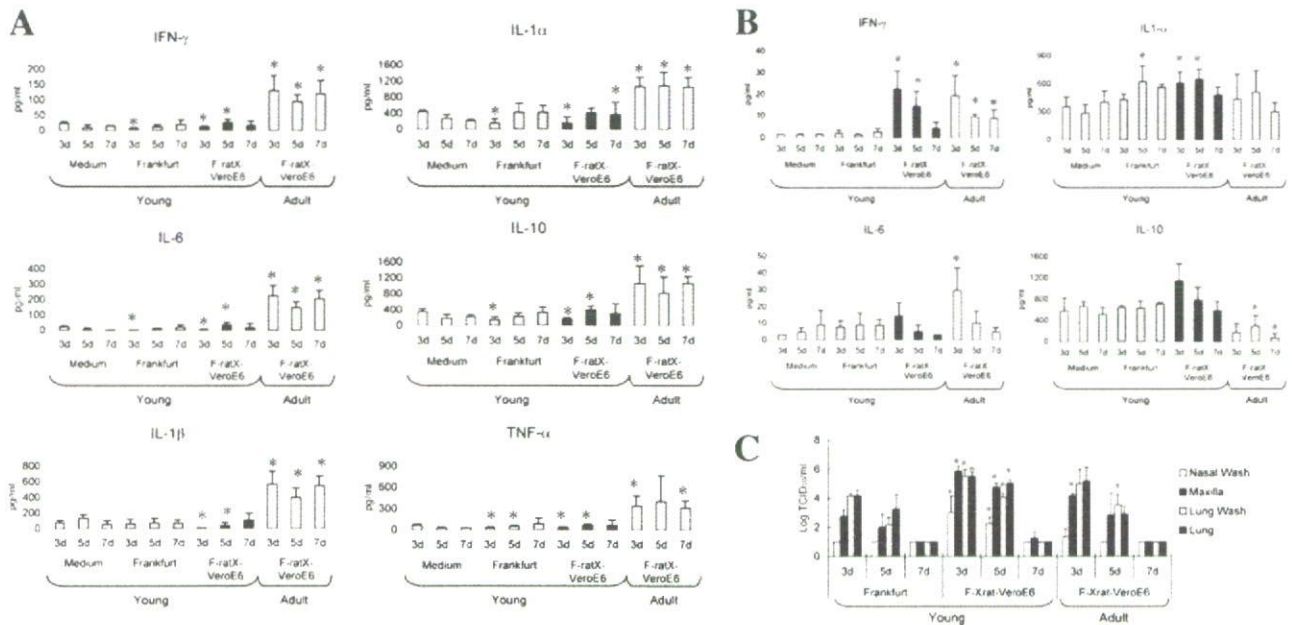


FIG. 4. Induction of inflammatory cytokines at the protein level in sera and lungs following SARS-CoV infection. (A) Cytokine levels in sera of F344 rats after infection. In F-ratX-VeroE6-inoculated adult rats ($n = 5$), serum levels of all cytokines were significantly higher than those seen in young rats ($n = 6$). Cytokine levels of adult F344 rats before infection ($n = 8$) were as follows: IFN- γ , 20.95 pg/ml; TNF- α , 183.77 pg/ml; IL-1 α , 371.71 pg/ml; IL-1 β , 33.64 pg/ml; IL-6, 22.54 pg/ml; IL-10, 47.07 pg/ml. (B) Cytokine levels in lung homogenates of young and adult F344 rats ($n = 3$) after infection. IFN- γ levels in F-ratX-VeroE6-inoculated young and adult rats were significantly higher than those seen in rats inoculated with the Frankfurt 1 isolate. IL-6 and IL-10 levels of F-ratX-VeroE6-inoculated adult rats were significantly higher and lower, respectively, than those seen in young rats. * $P < 0.05$ compared with medium-inoculated young F344 rats. (C) Virus titers of nasal and lung wash fluids and homogenates of maxilla including nasal cavity and lung of rats ($n = 3$) after infection. The detection limit was $10^{1.5}$ TCID₅₀/g of tissue.

macrophages. Fibrin deposition and hyaline membrane formation in alveolar ducts and alveoli were observed (Fig. 3F). By immunohistochemical staining, virus antigen-positive cells were alveolar macrophages and necrotic cells in the lesion (Fig. 3E to G, inset). There were no histopathological changes in the extrapulmonary tissues (brain, spinal cord, heart, liver, kidney, spleen, thymus, and gastrointestinal tract) of any of the animals examined. All the animals survived until the observation period.

Induction of cytokines in SARS-CoV-infected young and adult rats. To analyze the differences in pathogenicity seen in young and adult rats after infection with F-ratX-VeroE6, we examined cytokine levels in sera and lung homogenates (Fig. 4). Young F344 rats inoculated with medium containing 2% fetal bovine serum (100 μ l) or the Frankfurt 1 isolate (100 μ l of 10^7 TCID₅₀) served as controls. F-ratX-VeroE6 strain-infected adult rats showed significantly elevated levels of all 10 cytokines examined ($P < 0.05$) compared with mock-infected young rats (Fig. 4A). Levels of all 10 cytokines were also significantly different ($P < 0.05$) between young and adult rats infected with F-ratX-VeroE6. Adult rats showed elevated levels of IFN- γ ($P < 0.01$), IL-1 α ($P = 0.01$), IL-6 ($P < 0.01$), IL-10 ($P < 0.01$), IL-12 ($P < 0.01$), granulocyte-macrophage colony-stimulating factor ($P = 0.02$), IL-4 ($P < 0.01$), and IL-1 β ($P < 0.01$) after inoculation (P value between preinfected adult rats and F-ratX-VeroE6-infected adult rats on day 3 p.i.).

In lung homogenates, F-ratX-VeroE6-infected young and adult rats showed elevated levels of IFN- γ ($P = 0.012$ on day

3 and $P = 0.029$ on day 5 for young rats; $P = 0.031$ on day 3, $P < 0.01$ on day 5, and $P = 0.032$ on day 7 for adult rats) compared with mock-infected young rats (Fig. 4B). Elevated levels of IL-6 were observed early in infection in adult rats infected with F-ratX-VeroE6 compared with mock-infected rats ($P = 0.028$). Interestingly, IL-10 levels, which were significantly elevated in sera, decreased significantly in lung homogenates from adult rats infected with F-ratX-VeroE6 ($P = 0.046$ on day 5 and $P < 0.01$ on day 7 between mock-infected young rats; $P < 0.01$ on day 3, $P = 0.055$ on day 5, and $P = 0.009$ on day 7 between strain F-ratX-VeroE6-infected young rats).

Virus titers increased significantly ($P < 0.05$) in nasal and lung washes and in maxillar and lung homogenates of strain F-ratX-VeroE6-infected young rats on days 3 and 5 p.i. compared with strain Frankfurt 1-infected young rats (Fig. 4C). In contrast, in adult rats infected with the F-ratX-VeroE6 strain, virus titers increased significantly ($P < 0.05$) only in maxilla on day 3 p.i. and in lung washes on day 5 p.i. At day 7 p.i., the virus could not be isolated from the lungs of young and adult rats.

Introduction of a missense mutation within the ACE2 binding domain of the S protein of SARS-CoV during serial in vivo passage in rats. Immunohistochemical analyses revealed that ACE2 antigen-positive cells were found in respiratory epithelia of the trachea, bronchi, bronchioles, and alveolar cells of F344 rats (Fig. 5A). The ACE2 protein was most abundantly expressed on cilia of the trachea and intrapulmonary bronchus (Fig. 5A). ACE2 expression was also seen on the apical surface of bronchiolar cells and alveolar pneumocytes. During serial in vivo passage of SARS-CoV in F344 rats, virus replication sites

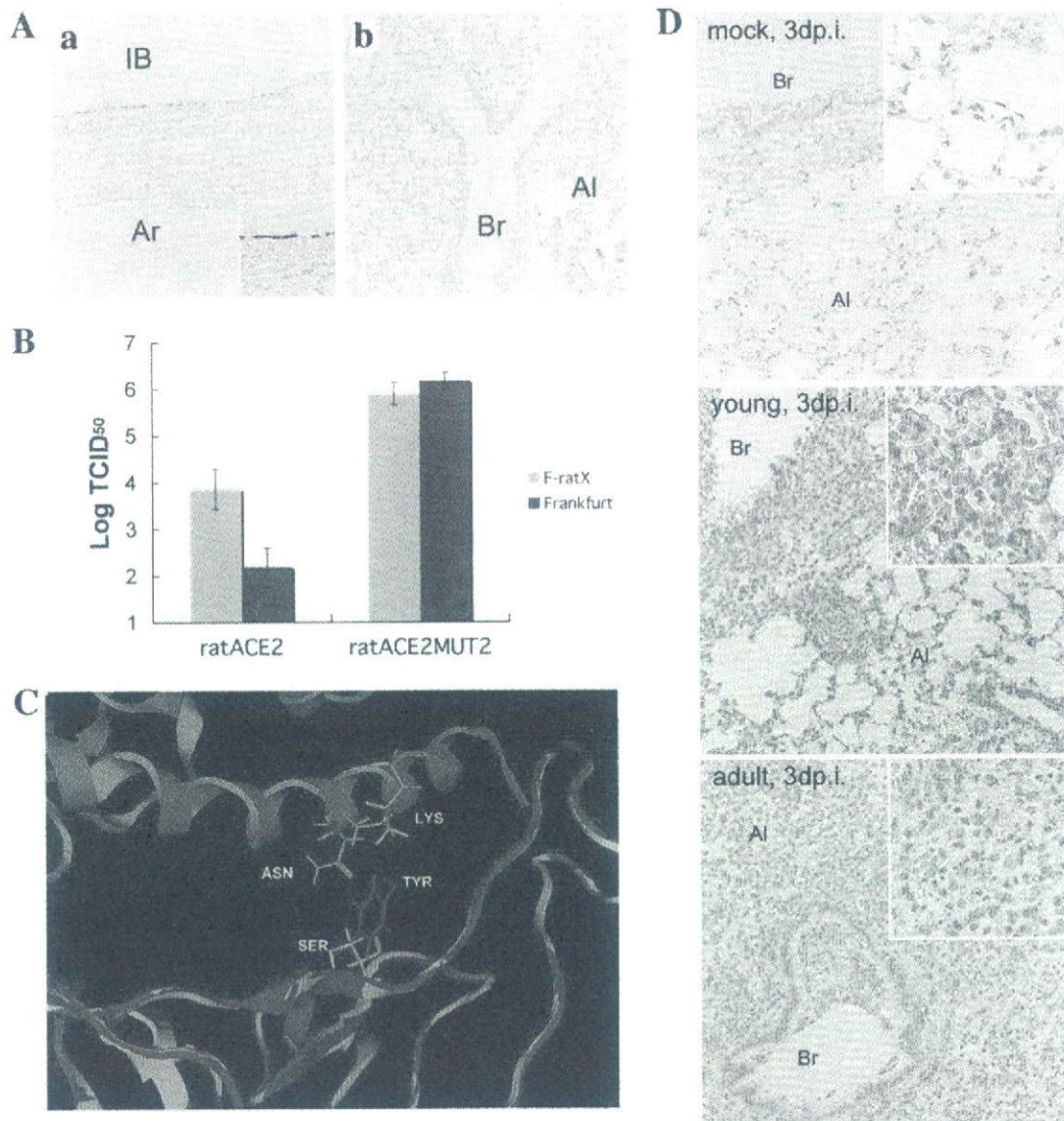


FIG. 5. Correlation of ACE2 expression and infection of serially passaged SARS-CoV in F344 rats. (A) ACE2 antigen-positive cells were detected on respiratory epithelia of the intrapulmonary bronchus (IB), bronchi (Br), and alveolar cells (Al) using immunohistochemical staining with anti-human ACE2 polyclonal antibody (magnification, $\times 50$; inset magnification, $\times 100$). (B) Binding of rat ACE2 to SARS-CoV in ACE2-expressing CHO cells. The F-ratX strain was detected at a higher titer than the Frankfurt 1 isolate in rat ACE2-expressing CHO cells (ratACE2) at 72 h p.i. Both Frankfurt 1 and F-ratX strains replicated in cells expressing variant forms of rat ACE2 in which residues 82 to 84 (NYS) were altered to human ACE2 (MYP) (ratACE2MUT2). The figure represents three experiments with similar results. (C) Molecular modeling of the rat-passaged SARS-CoV spike receptor binding domain complexed with rat ACE2. Green, rat ACE2; blue, Frankfurt 1 isolate; red, F-ratX strain. (D) Localization of ACE2 antigen-positive cells after infection with SARS-CoV on day 3 p.i. by staining with anti-human ACE2 polyclonal antibody. Br, bronchi; Al, alveoli. ACE2 antigen localized to alveolar cells and bronchial epithelial cells in lung of adult rats after mock infection (top, adult F344 rat after intranasal inoculation with MEM), ACE2 antigen-positive cells disappeared in affected bronchi of both young and adult rats (middle, young rat; bottom, adult F344 rat [both after intranasal inoculation with F-ratX-VeroE6]). High expression of ACE2 was found in the apical side of regenerated type II alveolar cells in lesion areas of young rats. Reduced ACE2 expression was observed in inflammatory areas of adult rats (magnification, $\times 50$; inset magnification, $\times 100$).

in lung extended from the bronchus to the alveolar area where ACE2-positive cells were located (Fig. 2 and 5A). ACE2 expression appeared to correlate with the extent and location of virus antigen-positive cells. To examine whether infection by rat-passaged virus is efficiently mediated by rat ACE2, F-ratX and the Frankfurt 1 isolate were inoculated onto rat ACE2-

expressing CHO cells. F-ratX replicated more efficiently in these cells than the Frankfurt 1 isolate, while both viruses replicated at the same level in CHO cells expressing an ACE2 variant in which amino acid residues 82 to 84 (NYS) were replaced by the corresponding MYP motif seen in human ACE2 (Fig. 5B). Sequence analysis of the F-ratX strain re-

vealed an A-to-C point mutation at nucleotide 1325 in the region encoding the ACE2 binding site of S1. This mutation resulted in a Y-to-S amino acid change at position 442 in the S protein. The 3-D structure of a complex of the receptor binding domain of the S protein and rat ACE2 predicts that the binding interface might be altered by such a mutation (Fig. 5C). ACE2 expression was examined by immunohistochemistry in young or adult rats after infection with F-ratX-VeroE6 (Fig. 5D). ACE2 antigen-positive cells disappeared in the affected bronchi of both young and adult rats. In young rats, however, ACE2 expression was seen in regenerated type II alveolar cells. By contrast, ACE2 antigen-positive cells were rarely observed in lung lesion areas of adult rats. Thus, ACE2 expression is highly downregulated in the F-ratX-VeroE6-infected adult rats.

DISCUSSION

Our goal was to understand the pathogenesis of SARS-CoV and develop an animal model of SARS. We demonstrated that serial *in vivo* passage of a human isolate of SARS-CoV, Frankfurt 1, in young F344 rats resulted in the increased virulence of SARS-CoV. The increased infectivity of SARS-CoV after serial passage in F344 rats was correlated with a single amino acid change in the receptor binding domain of the S1 protein, which mediates efficient SARS-CoV binding to ACE2 receptor-expressed rat cells based on both *in vitro* and structural studies. Adult F344 rats showed severe pathological changes compared with young F344 rats, and those changes were similar to features of human pathology recognized in the SARS epidemic of 2003 to 2004. Here, we demonstrate that both virus and host factors are crucial for the pathogenesis of SARS *in vivo*.

It has been reported that a virus variant in which 45 nucleotides (nucleotides 27670 to 27714) are deleted within ORF7b emerged upon replication of the Frankfurt 1 isolate in cell culture (37). Thus, for this study, we used a mixture of the original virus and the variant carrying the deletion. The observation that a variant with the deletion was detected in Frankfurt 1-infected rat specimens but was not detected following serial *in vivo* passaging suggests that the ORF7b may function in viral replication *in vivo*.

In addition, a Y-to-S amino acid change at residue 442 of the ACE2 binding domain of the S protein occurred during serial passage of the virus in F344 rats. As we have not yet completely sequenced all of the virus genome, it is still possible that another change enhanced virus replication in the rat. However, Li et al. previously demonstrated that residues 479N and 487T within the S-protein receptor binding domain are critical for efficient interaction with human ACE2 and that these residues might be introduced into the virus by mutations during the adaptation of palm civet SARS-CoV, which has 479K and 487S, to humans (20). It seems likely that the Y-to-S mutation at S-protein residue 442 is critical for efficient infection with rat ACE2, since F-ratX replicated more efficiently than the Frankfurt 1 isolate in rat ACE2-expressing CHO cells. Moreover, the 3-D structural prediction of a complex of the S-protein receptor binding domain and rat ACE2 suggests that the binding interface is altered by the Y-to-S mutation. Increased interactions may also be responsible for efficient replication of the

virus in rat, since during serial *in vivo* passage of the virus, replication sites in the lung extended from the bronchus, where ACE2 is most abundantly expressed, to the alveolar area, where it is expressed at a much lower level. Thus, the Y-to-S mutation at residue 442 may partly mediate the increased virulence seen in rats.

Based on immunohistochemical analysis of ACE2 expression in the lung of F344 rats, the ACE2 protein is most abundantly expressed on the cilia of trachea and intrapulmonary bronchi. ACE2 expression appears to correlate with the extent of virus replication sites. Upon infection with F-ratX-VeroE6, ACE2 antigen-positive cells disappeared in the affected bronchi of both young and adult rats. However, ACE2 was expressed in regenerated type II alveolar cells of young rats, but that expression was significantly reduced in adult rats. The downregulation of ACE2 expression by SARS-CoV infection and the presence of the SARS-CoV spike protein *in vivo* and *in vitro* have been previously reported (13). Since ACE2 negatively regulates the rennin-angiotensin system by inactivating angiotensin II, which is generated from angiotensin I by ACE, downregulation of ACE2 expression likely blocks the rennin-angiotensin pathway, which has a crucial role in severe acute lung injury (8, 13). Thus, the downregulation of ACE2 in the lungs of adult rats likely contributes to severe lung injury.

In F-ratX-VeroE6-infected young rats, more virus antigen-positive cells were found in the respiratory epithelia, including the alveolar area, with severe inflammatory reactions; however, rats did not show clinical symptoms of illness. On the other hand, adult rats showed clinical illness and severe pathological changes following F-ratX-VeroE6 infection. Such changes paralleled features seen in human pathologies following the SARS epidemic of the winter of 2003 to 2004 and strongly indicate that host as well as viral factors function in the pathogenesis of SARS in rats. Epidemiological studies of the SARS outbreak of 2003 to 2004 showed that advanced age was a risk factor for an adverse outcome from SARS (1, 3, 16, 27, 38). Roberts et al. previously demonstrated the efficiency of SARS-CoV replication in aged BALB/c mice (33). Our study of animals supports the observation that advanced age is a risk factor for the development of SARS.

Histopathological analysis of adult male F344 rats after F-ratX-VeroE6 infection showed severe inflammatory reactions, especially pulmonary edema. Furthermore, morphologically activated macrophages were observed in alveoli on days 3, 5, and 7 p.i. In contrast, after intranasal inoculation of young rats with F-ratX-VeroE6, inflammatory cell infiltrates consisted of leukocytes and lymphocytes on day 3 p.i. Acute lung injury caused by SARS-CoV is likely a complex pathophysiological process involving inflammatory cytokines released from activated macrophages in alveoli, leading to immune systems dysregulation (25). Our results suggest that the overinduction of inflammatory cytokines in sera and lung homogenates underlies the development of severe inflammation in adult rats. In lung homogenates in particular, IL-6 levels were increased significantly in adult rats after intranasal inoculation with F-ratX-VeroE6 on day 3 p.i.; however, IL-10 levels decreased significantly in adult rats on days 5 and 7 p.i. IL-6, an inflammatory cytokine, is produced by leukocytes, monocytes, endothelial cells, fibroblasts, and alveolar epithelial cells. Serum cytokine levels in SARS patients, particularly IL-6, are signif-

icantly elevated (40). In vitro studies suggest that SARS-CoV replication induces high levels of IL-6 compared with other respiratory viruses (26). Our findings indicate that IL-6 may be produced by predominantly infiltrated leukocytes and macrophages in injured lungs and leads to enhanced inflammatory reactions. By contrast, IL-10, an immunosuppressive cytokine of macrophages, Th2 lymphocytes, and B cells, inhibits TNF- α production and neutrophil activation in lipopolysaccharide-induced acute lung injury and leads to decreases in lung tissue injury (9). Therefore, decreased IL-10 levels in the lung may be responsible for the loss of protective mechanisms, enabling the inflammatory response to continue. It was reported that IL-10 levels increase in the convalescent phase in SARS patients (25). It is currently unclear why elevated cytokine levels are observed in adult rats following F-ratX-VeroE6 infection, since virus replication rates are decreased compared to those for infected young rats. However, our in vivo study suggests that excess cytokine activation may play a key role in the clinical and pathological features of SARS.

In conclusion, we developed an animal model of SARS after SARS-CoV was passaged 10 times in F344 rats and then propagated in Vero E6 cells (F-ratX-VeroE6). This study suggests that both virus and host factors underlie the pathogenesis of SARS. Such an in vivo comparative study of immune responses of young and adult rats using the adapted virus could be useful in further understanding the pathogenesis of SARS, and this model described here should be useful to evaluate vaccine candidates and antiviral agents against SARS-CoV infection.

ACKNOWLEDGMENTS

We thank J. Ziebuhr, Institute of Virology and Immunology, University of Würzburg, Würzburg, Germany, for kindly supplying the Frankfurt 1 isolate. We also thank M. Fujino, I. Hatano, and M. Kataoka, Department of Pathology, National Institute of Infectious Diseases, for technical assistance.

This work was partly supported by a Grant-in Aid for Research on Emerging and Re-Emerging Infectious Diseases from the Ministry of Health, Labor, and Welfare, Japan, and a Grant-in-Aid for Scientific Research from the Ministry of Education, Culture, Sports, Science, and Technology, Japan.

REFERENCES

- Booth, C. M., L. M. Matukas, G. A. Tomlinson, A. R. Rachlis, D. B. Rose, H. A. Dwosh, S. L. Walmsley, T. Mazzulli, M. Avendano, P. Derkach, I. E. Eptimios, I. Kitai, B. D. Mederski, S. B. Shadowitz, W. L. Gold, L. A. Hawryluck, E. Rea, J. S. Chenkin, D. W. Cescon, S. M. Poutanen, and A. S. Detsky. 2003. Clinical features and short-term outcomes of 144 patients with SARS in the greater Toronto area. *JAMA* **289**:2801–2809.
- Bukreyev, A., E. W. Lamirande, U. J. Buchholz, L. N. Vogel, W. R. Elkins, M. St. Claire, B. R. Murphy, K. Subbarao, and P. L. Collins. 2004. Mucosal immunisation of African green monkeys (*Cercopithecus aethiops*) with an attenuated parainfluenza virus expressing the SARS coronavirus spike protein for the prevention of SARS. *Lancet* **363**:2122–2127.
- Donnelly, C. A., A. C. Ghani, G. M. Leung, A. J. Hedley, C. Fraser, S. Riley, L. J. Abu-Raddad, L. M. Ho, T. Q. Thach, P. Chau, K. P. Chan, T. H. Lam, L. Y. Tse, T. Tsang, S. H. Liu, J. H. Kong, E. M. Lau, N. M. Ferguson, and R. M. Anderson. 2003. Epidemiological determinants of spread of causal agent of severe acute respiratory syndrome in Hong Kong. *Lancet* **361**:1761–1766.
- Drosten, C., S. Günther, W. Preiser, S. van der Werf, H. R. Brodt, S. Becker, H. Rabenau, M. Panning, L. Kolesnikova, R. A. M. Fouchier, A. Berger, A. M. Burguière, J. Cinatl, M. Eickmann, N. Escriviou, K. Grywna, S. Kramme, J. C. Mariuerra, S. Müller, V. Rickerts, M. Stürmer, S. Vieth, H. D. Klenk, A. D. M. E. Osterhaus, H. Schmitz, and H. W. Doerr. 2003. Identification of a novel coronavirus in patients with severe acute respiratory syndrome. *N. Engl. J. Med.* **348**:1967–1976.
- Fouchier, R. A. M., T. Kuiken, M. Schutten, G. van Amerongen, G. J. J. van Doornum, B. G. van den Hoogen, M. Peiris, W. Lim, K. Stöhr, and A. D. M. E. Osterhaus. 2003. Koch's postulates fulfilled for SARS virus. *Nature* **423**:240.
- Gao, W., A. Tamin, A. Soloff, L. D'Auto, E. Swanegbo, P. D. Robbins, W. J. Bellini, S. Barratt-Boyes, and A. Gambotto. 2003. Effects of a SARS-associated coronavirus vaccine in monkeys. *Lancet* **362**:1895–1896.
- Greenough, T. C., A. Carville, J. Coderre, M. Somasundaran, J. L. Sullivan, K. Luzuriaga, and K. Mansfield. 2005. Pneumonitis and multi-organ system disease in common marmosets (*Callithrix jacchus*) infected with the severe acute respiratory syndrome-associated coronavirus. *Am. J. Pathol.* **167**:455–463.
- Imai, Y., K. Kuba, S. Rao, Y. Huan, F. Guo, B. Guan, P. Yang, R. Sarao, T. Wada, H. Leong-Poi, M. A. Crackower, A. Fukamizu, C. C. Hui, L. Hein, S. Uhlig, A. S. Slutsky, C. Jiang, and J. M. Penninger. 2005. Angiotensin-converting enzyme 2 protects from severe acute lung failure. *Nature* **436**:112–116.
- Inoue, G. 2000. Effect of interleukin-10 (IL-10) on experimental LPS-induced acute lung injury. *J. Infect. Chemother.* **6**:51–60.
- Jia, H. P., D. C. Look, L. Shi, M. Hickey, L. Pewe, J. Netland, M. Farzan, C. Wohlford-Lenane, S. Perlman, and P. B. McCray, Jr. 2005. ACE2 receptor expression and severe acute respiratory syndrome coronavirus infection depend on differentiation of human airway epithelia. *J. Virol.* **79**:14614–14621.
- Kinoshita, M., M. Yokoyama, H. Sato, A. Kojima, T. Kurata, K. Ikuta, T. Sata, and K. Tokunaga. 2005. Amino acid 36 in the human immunodeficiency virus type 1 gp120 ectodomain controls fusogenic activity: implications for the molecular mechanism of virus escape from a fusion inhibitor. *J. Virol.* **79**:5996–6004.
- Ksiazek, T. G., D. Erdman, C. S. Goldsmith, S. R. Zaki, T. Peret, S. Emery, S. Tong, C. Urbani, J. A. Comer, W. Lim, P. E. Rollin, S. F. Dowell, A.-E. Ling, C. D. Humphrey, W.-J. Shieh, J. Guarner, C. D. Paddock, P. Rota, B. Fields, J. DeRisi, J. Y. Yang, N. Cox, J. M. Hughes, J. W. LeDuc, W. J. Bellini, L. J. Anderson, and the SARS Working Group. 2003. A novel coronavirus associated with severe acute respiratory syndrome. *N. Engl. J. Med.* **348**:1953–1966.
- Kuba, K., Y. Imai, S. Rao, H. Gao, F. Guo, B. Guan, Y. Huan, P. Yang, Y. Zhang, W. Deng, L. Bao, B. Zhang, G. Liu, Z. Wang, M. Chappell, Y. Liu, D. Zheng, A. Leibbrandt, T. Wada, A. S. Slutsky, D. Liu, C. Qin, C. Jiang, and J. M. Penninger. 2005. A crucial role of angiotensin converting enzyme 2 (ACE2) in SARS coronavirus-induced lung injury. *Nat. Med.* **11**:875–879.
- Kuiken, T., R. A. M. Fouchier, M. Schutten, G. F. Rimmelzwaan, G. van Amerongen, D. van Riel, J. D. Laman, T. de Jong, G. van Doornum, W. Lim, A. E. Ling, P. K. S. Chan, J. S. Tam, M. C. Zambon, R. Gopal, C. Drosten, S. van der Werf, N. Escriviou, J. C. Manuerra, K. Stöhr, J. S. M. Peiris, and A. D. M. E. Osterhaus. 2003. Newly discovered coronavirus as the primary cause of severe acute respiratory syndrome. *Lancet* **362**:263–270.
- Lai, M. C., and K. V. Holmes. 2001. Coronaviridae: the viruses and their replication, p. 1163–1185. In D. M. Knipe and P. M. Howley (ed.), *Fields virology*, 4th ed. Lippincott Williams & Wilkins, Philadelphia, PA.
- Lee, N., D. Hui, A. Wu, P. Chan, P. Cameron, G. M. Joynt, A. Abuja, M. Y. Yung, B. Sc, C. B. Leung, K. F. To, S. F. Lui, C. C. Szeto, S. Chung, and J. J. Y. Sung. 2003. A major outbreak of severe acute respiratory syndrome in Hong Kong. *N. Engl. J. Med.* **348**:1986–1994.
- Li, B. J., Q. Tang, D. Cheng, C. Qin, F. Y. Xie, Q. Wei, J. Xu, Y. Liu, B. J. Zheng, M. C. Woodle, N. Zhong, and P. Y. Lu. 2005. Using siRNA in prophylactic and therapeutic regimens against SARS coronavirus in Rhesus macaque. *Nat. Med.* **9**:944–951.
- Li, F., W. Li, M. Farzan, and S. C. Harrison. 2005. Structure of SARS coronavirus spike receptor-binding domain complexed with receptor. *Science* **309**:1864–1868.
- Li, W., M. J. Moore, N. Vasilieva, J. Sui, S. K. Wong, M. A. Berne, M. Somasundaran, J. L. Sullivan, K. Luzuriaga, T. C. Greenough, H. Choe, and M. Farzan. 2003. Angiotensin-converting enzyme 2 is a functional receptor for the SARS coronavirus. *Nature* **426**:450–454.
- Li, W., C. Zhang, J. Sui, J. H. Kuhn, M. J. Moore, S. Luo, S. K. Wong, I. C. Huang, K. Xu, N. Vasilieva, A. Murakami, Y. He, W. A. Marasco, Y. Guan, H. Choe, and M. Farzan. 2005. Receptor and viral determinants of SARS-coronavirus adaptation to human ACE2. *EMBO J.* **24**:1634–1643.
- Li, W., T. C. Greenough, M. J. Moore, N. Vasilieva, M. Somasundaran, J. L. Sullivan, M. Farzan, and H. Choe. 2004. Efficient replication of severe acute respiratory syndrome coronavirus in mouse cells is limited by murine angiotensin-converting enzyme 2. *J. Virol.* **78**:11429–11433.
- Liang, L., C. He, M. Lei, S. Li, Y. Hao, H. Zhu, and Q. Duan. 2005. Pathology of guinea pigs experimentally infected with a novel reovirus and coronavirus isolated from SARS patients. *DNA Cell Biol.* **24**:485–490.
- Martina, B. E., B. L. Haagmans, T. Kuiken, R. A. Fouchier, G. F. Rimmelzwaan, G. Van Amerongen, J. S. Peiris, W. Lim, and A. D. Osterhaus. 2003. SARS virus infection of cats and ferrets. *Nature* **425**:915.
- McAuliffe, J. L., L. Vogel, A. Roberts, G. Fahle, S. Fischer, W. Shieh, E. Butler, S. Zaki, M. S. Claire, B. Murphy, and K. Subbarao. 2004. Replication of SARS coronavirus administered into the respiratory tract of African green rhesus and cynomolgus monkeys. *Virology* **330**:8–15.
- Nicholls, J. M., L. L. Poon, K. C. Lee, W. F. Ng, S. T. Lai, C. Y. Leung, C. M. Chu, P. K. Hui, K. L. Mak, W. Lim, K. W. Yan, K. H. Chan, N. C. Tsang, Y.

- Guan, K. Y. Yuen, and J. S. Peiris. 2003. Lung pathology of fatal severe acute respiratory syndrome. *Lancet* **361**:1773–1778.
26. Okabayashi, T., H. Kariwa, S. Yokota, S. Iki, T. Indoh, N. Yokosawa, I. Takashima, H. Tsutsumi, and N. Fujii. 2006. Cytokine regulation in SARS coronavirus infection compared to other respiratory virus infections. *J. Med. Virol.* **78**:417–424.
 27. Peiris, J. S., C. M. Chu, V. C. Cheng, K. S. Chan, I. F. Hung, L. L. Poon, K. L. Law, B. S. Tang, T. Y. Hon, C. S. Chan, K. H. Chan, J. S. Ng, B. J. Zheng, W. L. Ng, R. W. Lai, Y. Guan, K. Y. Yuen, and the HKU/UCH SARS Study Group. 2003. Clinical progression and viral load in a community outbreak of coronavirus-associated SARS pneumonia: a prospective study. *Lancet* **361**:1767–1772.
 28. Peiris, J. S. M., S. T. Lai, L. L. M. Poon, Y. Guan, L. Y. C. Yam, W. Lim, J. Nicholls, W. K. S. Yee, W. W. Yan, M. T. Cheung, V. C. C. Cheng, K. H. Chan, D. N. C. Tsang, R. W. H. Yung, T. K. Ng, K. Y. Yuen, and Members of the SARS Study Group. 2003. Coronavirus as a possible cause of severe acute respiratory syndrome. *Lancet* **361**:1319–1325.
 29. Ponder, J. W., and D. A. Case. 2003. Force fields for protein simulations. *Adv. Protein Chem.* **66**:27–85.
 30. Qin, C., J. Wang, Q. Wei, M. She, W. A. Marasco, H. Jiang, X. Tu, H. Zhu, L. Ren, H. Gao, L. Guo, L. Huang, R. Yang, Z. Cong, L. Guo, Y. Wang, Y. Liu, Y. Sun, S. Duan, J. Qu, L. Chen, W. Tong, L. Ruan, P. Liu, H. Zhang, J. Zhang, H. Zhang, D. Liu, Q. Liu, T. Hong, and W. He. 2005. An animal model of SARS produced by infection of *Macaca mulatta* with SARS coronavirus. *J. Pathol.* **206**:251–259.
 31. Qin, E., H. Shi, L. Tang, C. Wang, G. Chang, Z. Ding, K. Zhao, J. Wang, Z. Chen, M. Yu, B. Si, J. Liu, D. Wu, X. Cheng, B. Yang, W. Peng, Q. Meng, B. Liu, W. Han, X. Yin, H. Duan, D. Zhan, L. Tian, S. Li, J. Wu, G. Tan, Y. Li, Y. Li, Y. Liu, H. Liu, F. Lv, Y. Zhang, X. Kong, B. Fan, T. Jiang, S. Xu, X. Wang, C. Li, X. Wu, Y. Deng, M. Zhao, and Q. Zhu. 2005. Immunogenicity and protective efficacy in monkeys of purified inactivated Vero-cell SARS vaccine. *Vaccine* **24**:1028–1034.
 32. Roberts, A., L. Vogel, J. Guarner, N. Hayes, B. Murphy, S. Zaki, and K. Subbarao. 2005. Severe acute respiratory syndrome coronavirus infection of golden Syrian hamsters. *J. Virol.* **79**:503–511.
 33. Roberts, A., C. Paddock, L. Vogel, E. Butler, S. Zaki, and K. Subbarao. 2005. Aged BALB/c mice as a model for increased severity of severe acute respiratory syndrome in elderly humans. *J. Virol.* **79**:5833–5838.
 34. Rowe, T., G. Gao, R. J. Hogan, R. G. Crystal, T. G. Voss, R. L. Grant, P. Bell, G. P. Kobinger, N. A. Wivel, and J. M. Wilson. 2004. Macaque model for severe acute respiratory syndrome. *J. Virol.* **78**:11401–11404.
 35. Sims, A. C., R. S. Baric, B. Yount, S. E. Burkett, P. L. Collins, and R. J. Pickles. 2005. Severe acute respiratory syndrome coronavirus infection of human ciliated airway epithelia: role of ciliated cells in viral spread in the conducting airways of the lungs. *J. Virol.* **79**:15511–15524.
 36. Snijder, E. J., P. J. Bredenbeek, J. C. Dobbe, V. Thiel, J. Ziebuhr, L. L. Poon, Y. Guan, M. Rozanov, W. J. Spaan, and A. E. Gorbalenya. 2003. Unique and conserved features of genome and proteome of SARS-coronavirus, an early split-off from the coronavirus group 2 lineage. *J. Mol. Biol.* **331**:991–1004.
 37. Thiel, V., K. A. Ivanov, A. Putics, T. Hertzog, B. Schelle, S. Bayer, B. Weissbrich, E. J. Snijder, H. Rabenau, H. W. Doerr, A. E. Gorbalenya, and J. Ziebuhr. 2003. Mechanisms and enzymes involved in SARS coronavirus genome expression. *J. Gen. Virol.* **84**:2305–2315.
 38. Tsui, P. T., M. L. Kwok, H. Yuen, and S. T. Lai. 2003. Severe acute respiratory syndrome: clinical outcome and prognostic correlates. *Emerg. Infect. Dis.* **9**:1064–1069.
 39. Weingartl, H. M., J. Copps, M. A. Drebot, P. Marszal, G. Smith, J. Gren, M. Andova, J. Pasick, P. Kitching, and M. Czub. 2004. Susceptibility of pigs and chickens to SARS coronavirus. *Emerg. Infect. Dis.* **10**:179–184.
 40. Zhang, Y., J. Li, Y. Zhan, L. Wu, X. Yu, W. Zhang, L. Ye, S. Xu, R. Sun, Y. Wang, and J. Lou. 2004. Analysis of serum cytokines in patients with severe acute respiratory syndrome. *Infect. Immun.* **72**:4410–4415.

Rapid Genome Sequencing of RNA Viruses

Tetsuya Mizutani,* Daiji Endoh,†
 Michiko Okamoto,‡ Kazuya Shirato,*
 Hiroyuki Shimizu,* Minetaro Arita,*
 Shuetsu Fukushi,* Masayuki Saijo,*
 Kouji, Sakai,* Chang Kweng Lim,* Mikako Ito,*
 Reiko Nerome,* Tomohiko Takasaki,* Koji Ishii,*
 Tetsuro Suzuki,* Ichiro Kurane,*
 Shigeru Morikawa,* and Hidekazu Nishimura‡

We developed a system for rapid determination of viral RNA sequences whereby genomic sequence is obtained from cultured virus isolates without subcloning into plasmid vectors. This method affords new opportunities to address the challenges of unknown or untypeable emerging viruses.

Over the past few years, global migration has led to emerging infectious diseases that pose substantial risks to public health. To prevent potential outbreaks, early detection of infectious pathogens is necessary. In particular, the recent outbreak of severe acute respiratory syndrome (SARS) provided important lessons on how unknown viruses should be detected rapidly. Thus, a standardized and qualified system is required for rapid nucleic acid sequence determination for newly emerging viruses.

Recently, we developed a new method for detecting RNA viruses. This method, based on cDNA representational difference analysis (cDNA RDA), uses 96 hexanucleotides that are not suitable for priming ribosomal RNAs but that normally prime most of the genome of an RNA virus as primers for reverse transcription in cDNA RDA (1). However, the RDA method with a cloning step requires at least 1 week for the determination of the nucleic acid sequence.

The Method

Our new system for rapid determination of viral RNA sequence (RDV) uses whole-genome amplification and direct sequencing techniques (Figure 1). The RDV method comprises 6 procedures: 1) effective destruction of cellular RNA and DNA for semipurification of viral particles, 2) effective elimination of DNA fragments by using a pre-

filtration column system and elution of small amounts of RNA, 3) effective synthesis of first- and second-strand cDNAs, 4) construction and amplification of a cDNA library, 5) construction of a second cDNA library, and 6) direct sequencing using optimized primers. The RDV method enables a broad range of partial nucleotide sequences within the entire viral RNA genome to be obtained within 2 days without cloning into plasmids.

To eliminate contaminating cellular RNA and DNA from the samples, 0.001 µg of RNase A (Qiagen, Hilden, Germany) and 1 µL (2 U) of Turbo DNA-free DNase I (Ambion, Austin, TX, USA) with 1× Turbo DNA-free buffer were incubated at 37°C for 30 min under conditions that prevented destruction of viral RNA in the viral particles. The RNA in the viral particles was then extracted within 30 min by using a total RNA isolation mini kit (Agilent Technologies Inc., Palo Alto, CA, USA). We confirmed that DNA was effectively eliminated by this RNA extraction kit.

In accordance with the Invitrogen manual, cDNA was synthesized, by using random hexamers (Takara Bio Inc., Kyoto, Japan) and Superscript III (Invitrogen, Carlsbad, CA, USA) lacking RNase H activity, at 50°C for 1 h. Then 60 U of RNase H (Takara Bio Inc.) added before synthesis of second-strand cDNA at 50°C for 1 h. In accordance with the manual, a whole genome amplification system (WGA; Sigma-Aldrich, Saint Louis, MO, USA), which was developed for amplification of genomic DNA, was used to amplify viral double-stranded cDNA. This process was

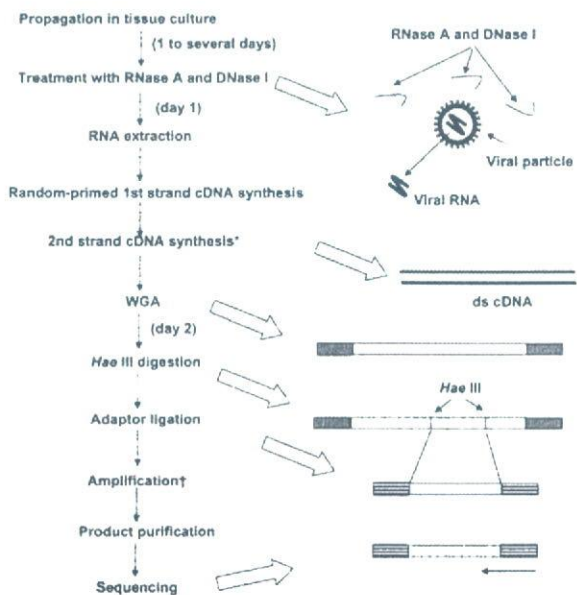


Figure 1. Overall scheme of the rapid determination of viral RNA sequence method. *By adding RNase H; WGA, whole genome amplification; †With specially designed primer sets as shown in Figure 2.

*National Institute of Infectious Diseases, Tokyo, Japan; †Rakuno Gakuen University, Ebetsu, Japan; and ‡Sendai Medical Center, Sendai, Japan

performed within 90 min. Instead of the Taq polymerase recommended in the kit, we used 1.25 U of AmpliTaq Gold LD (Applied Biosystems, Foster City, CA, USA) to obtain a high yield of the PCR products. Primers were provided in the WGA kit, but no information regarding their sequences was obtained. The reaction mixture was heated at 95°C for 9 min (for activation of AmpliTaq Gold), followed by 70 cycles of amplification using Mastercycler (Eppendorf AG, Hamburg, Germany). Each PCR cycle consisted of annealing at 68°C for 1 min, primer extension at 72°C for 5 min, and denaturation at 94°C for 1 min.

The 1st cDNA library was digested with 40 U of *Hae*III (Takara Bio Inc.) at 37°C for 30 min. DNA was purified by using the MonoFas DNA isolation system (GL Science, Tokyo, Japan), and a blunt *Eco*RI-*Not*I-*Bam*HI adaptor (10 pmol; Takara Bio Inc.) was ligated at 16°C for 30 min by using DNA Ligation Kit, Mighty Mix (Takara Bio Inc.). The second cDNA library was amplified by PCR with specially designed primer sets in which 6 nucleotides composed of CC (*Hae*III-digested sequence) and 4 variable nucleotides were added to the 3' end of the adaptor sequence (Figure 2). For example, 1 primer set was as follows: forward primer, H1-1: 5'-AATTCGGCGGCCGGATCCCCGGG-3'; reverse primer H9-3: 5'-AATTCGGCGGCCGGATCCCCAGGA-3' (the adaptor sequence is underlined, and the *Hae*III-digested sequence is shown in italics) (Figure 2).

We always used >12 primer sets and 0.83 μmol of each primer per cDNA library. PCR was performed with AmpliTaq Gold Master Mix (Applied Biosystems). The reaction mixture was heated at 95°C for 12 min, followed by 70 cycles of amplification. Each PCR cycle consisted of annealing and primer extension at 72°C for 30 s and denaturation at 94°C for 30 s. A single band was consistently obtained in ≈50% of the reactions. DNA was purified from the PCR by using MonoFas. Occasionally, we purified DNA fragments from the gels when >2 bands were detected. Direct sequencing was performed with the forward primer, reverse primer, or both.

When the number of viral particles in the sample was high, we omitted the RNase A and DNase I treatments and used the RNeasy Mini Kit (Qiagen) for RNA extraction. We occasionally used a whole transcriptome amplification kit (Rubicon Genomics Inc, Ann Arbor, MI, USA) instead of the WGA kit because both kits yielded similar amplification results.

In preliminary studies that used referential RNA viruses, we attempted to determine the nucleic acid sequences of SARS coronavirus, mouse hepatitis virus, West Nile virus, Japanese encephalitis virus, and dengue virus type 2 in culture supernatants (10–100 μL) by using the RDV method. The percentages of positive fragments (number of fragments containing viral nucleic acid/total number of

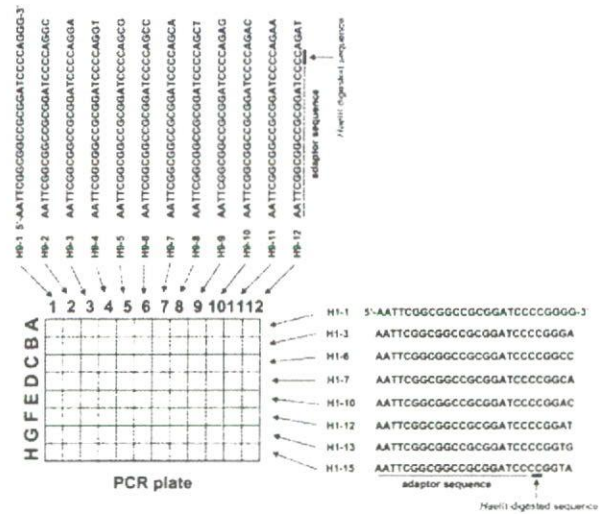


Figure 2. Primers used in rapid determination of viral RNA sequence method.

sequenced fragments) in the reactions for detection of these 5 viruses were 60% (3/5), 45% (5/11), 100% (12/12), 50% (5/10), and 40% (4/10), respectively. As a clinical application, a throat swab specimen from a patient with fever and upper respiratory infection was characterized. Although the specimen exhibited enterovirus-like cytopathic effect by inoculation into HEF and GMK cells when cell culture system for virus isolation was used (2), extracted RNA from the supernatant of the cells showed no amplification by reverse transcription-PCR (RT-PCR) when 1 of the conventional primer sets for human enteroviruses was used (3,4). In the cell culture supernatant analysis by the RDV method, the specimen exhibited amplification of the partial nucleotide sequences of coxsackie A14 virus (nucleotide sequence data are available in the DDBJ/EMBL/GenBank databases under accession nos. AB275848–AB275853). Thus, the RDV method could detect unidentified cytopathic-effect agents such as enterovirus that could not be detected by RT-PCR when the conventional primer set for enteroviruses was used.

Conclusions

The RDV method is a rapid method for the direct determination of viral RNA sequences without using the cDNA cloning procedure. The limitations of the RDV method are the requirement for cell culture isolate and the large number of steps. However, RDV would be useful for species-independent detection of RNA viruses including unknown or untypeable emerging RNA viruses. Furthermore, with minor modifications, this method would also be applicable to the detection of DNA viruses and bacteria.

Acknowledgments

We thank F. Taguchi and R. Watanabe for helpful discussions and M. Ogata for assistance.

This work was supported in part by the Japan Society for Promotion of Science, Tokyo, Japan.

Dr Mizutani is a senior researcher at the National Institute of Infectious Diseases, Tokyo, Japan. His current research focus is infectious disease surveillance by using new technologies.

References

1. Endoh D, Mizutani T, Kirisawa R, Maki Y, Saito H, Kon Y, et al. Species-independent detection of RNA virus by representational difference analysis using non-ribosomal hexanucleotides for reverse transcription. *Nucleic Acids Res.* 2005;33:e65.
2. Numazaki Y, Oshima T, Ohmi A, Tanaka A, Oizumi Y, Komatsu S, et al. A microplate method for isolation of viruses from infants and children with acute respiratory infections. *Microbiol Immunol.* 1987;31:1085-95.
3. Olive DM, Al-Mufti S, Al-Mulla W, Khan MA, Pasca A, Stanway G, et al. Detection and differentiation of picornaviruses in clinical samples following genomic amplification. *J Gen Virol.* 1990;71:2141-7.
4. Ishiko H, Shimada Y, Yonaha M, Hashimoto O, Hayashi A, Sakae K, et al. Molecular diagnosis of human enteroviruses by phylogeny-based classification by use of the VP4 sequence. *J Infect Dis.* 2002;185:744-54.

Address for correspondence: Tetsuya Mizutani, Department of Virology I, National Institute of Infectious Diseases, Gakuen 4-7-1, Musashimurayama City, Tokyo 208-0011, Japan; email: tmizutan@nih.go.jp

Rapid Communication

An improved procedure for rapid determination of viral RNA sequences of avian RNA viruses

K. Sakai¹, T. Mizutani¹, S. Fukushi¹, M. Saijo¹, D. Endoh², I. Kurane¹, K. Takehara³, S. Morikawa¹

¹ Department of Virology 1, National Institute of Infectious Diseases, Tokyo, Japan

² Laboratory of Veterinary Radiology, School of Veterinary Medicine, Rakuno Gakuen University, Ebetsu, Japan

³ Laboratory of Zoonoses, School of Veterinary Medicine and Animal Sciences, Kitasato University, Towada, Aomori, Japan

Received 19 March 2007; Accepted 27 April 2007; Published online 1 June 2007

© Springer-Verlag 2007

Summary

A system for rapid determination of viral RNA sequences, RDV, was improved for detection of avian RNA virus in allantoic fluids. We detected avian paramyxovirus nucleotide sequences using RDV method ver 2.0.

There have been a number of recent outbreaks of avian influenza and West Nile virus spread *via* birds. Assays based on molecular diagnostics, such as polymerase chain reaction (PCR), are now available. However, PCR is not available for unknown emerging infectious viral diseases because of the lack of nucleic acid sequence data. Therefore, a system for rapid nucleic acid sequence determination is required for newly emerging viruses spread *via* birds.

Recently, we developed two new methods for the detection of RNA viruses, one of which is based on cDNA representational difference analysis (cDNA

RDA) using 96 hexanucleotides that do not prime ribosomal RNAs but prime most RNA viral genomes at the reverse transcription step [2]. However, this method requires at least one week for determination of the nucleic acid sequence. The other method is a system for rapid determination of viral RNA sequences (RDV method) [3], which uses whole-genome amplification and direct sequencing techniques. The RDV method enables a broad range of partial nucleotide sequences of viral RNA genomes to be obtained within 2 days without cloning. We succeeded in determining the nucleic acid sequences of severe acute respiratory syndrome coronavirus, mouse hepatitis virus, West Nile virus, Japanese encephalitis virus, and dengue virus type 2 in culture supernatants using the RDV method [3]. However, the limitation of this method is the requirement for supernatant of virus-infected cultured cells as a starting material. In the present study, we demonstrate the application of this method to avian RNA virus from allantoic fluid because many viruses spread *via* birds have been diagnosed by virus isolation using inoculation of embryonated chicken eggs. We have improved the

Correspondence: Tetsuya Mizutani, Ph.D., Department of Virology 1, National Institute of Infectious Diseases, 1-23-1 Toyama, Shinjuku-ku, Tokyo 162-8640, Japan
e-mail: tmizutan@nih.go.jp

previously reported RDV method (renamed RDV method ver 1.0) with regard to synthesis of cDNA, double-stranded DNA, and amplification to increase sensitivity.

A fecal sample was collected from northern pintail (*Anas acuta*) at Lake Izunuma-Uchinuma in Tohoku district, northeast Japan. The sample was placed into PBS containing antibiotics to give a 30% suspension. The suspension was centrifuged and the supernatant was inoculated into the allantoic cavities of 10-day-old chicken embryos. The eggs were incubated for 3 days. At the end of the incubation period, the allantoic fluids were taken and tested for hemagglutination activity with 0.5% chicken red blood cells. The allantoic fluids showed hemagglutination activity; however, they were not identified as Newcastle disease virus nor avian influenza A virus.

RNA was first extracted from the allantoic fluids using Isogen-LS (Nippon Gene, Tokyo, Japan) and then extracted using a total RNA isolation mini kit (Agilent Technologies Inc., Palo Alto, CA, USA). A whole transcriptome amplification system (WTA; Sigma-Aldrich, Saint Louis, MO, USA) was used to amplify viral double-stranded cDNA in accordance with the manufacturer's instructions. Instead of the Taq polymerase recommended in the kit, we used 25 μ l of multiplex PCR mix 2 containing reaction buffer, 0.25 μ l of multiplex PCR mix 1 containing Taq polymerase (Takara Bio Inc., Shiga, Japan), WTA master mix containing primers (Sigma-Aldrich: no information regarding their sequences), and 2.5 μ l of cDNA in a total volume of 50 μ l to obtain PCR products in high yield. The reaction mixture was heated at 94 °C for 60 sec, followed by 40 cycles of amplification using a Mastercycler (Eppendorf AG, Hamburg, Germany). Each PCR cycle consisted of annealing at 65 °C for 90 sec, primer

extension at 72 °C for 90 sec, and denaturation at 94 °C for 30 sec. The results of preliminary experiments confirmed that this modified method, RDV ver 2.0, increased sensitivity compared with the previous protocol, RDV ver 1.0 (data not shown).

After the first cDNA library was digested with *Hae*III and ligated with a blunt *Eco*RI-*Not*I-*Bam*HI adaptor, the second cDNA library was amplified by PCR with specially designed primer sets as follows: forward primer, H1-5: 5'-AATTCGGCGGCCGCGGATCCCCGGCG-3'; reverse primer H9-1: 5'-AATTCGGCGGCCGCGGATCCCCAGGA-3' or H9-2, -3, -4, -5, -6, -7, -8, -9, -10, -11 (described in ref. [3]) and -13 (AATTCGGCGGCCGCGGA TCCCCAGTG) (the adaptor sequence is underlined, and the *Hae*III-digested sequence is shown in italics). Direct sequencing was performed with the forward primer, H1-5.

Four of fifteen DNA fragments were closely related to avian paramyxovirus (APMV) type 6 designated APMV-6/duck/Taiwan/Y1/98 (accession no. AY029299) [1]. Figure 1 shows the locations of PCR fragments on the genome of APMV. To confirm that the RNA specimen contained genomic RNA of APMV, we designed primer sets corresponding to the large (L) region of APMV (approximately 1.1 kb) for reverse transcription (RT)-PCR based on the sequence deposited in GenBank (accession no. AY029299), and RT-PCR was performed using SuperScript III (Invitrogen, San Diego, CA, USA) for RT and the Expand High Fidelity PCR system (Roche, Mannheim, Germany) for PCR. We obtained a single band at 1.1 kb (data not shown) and determined the nucleic acid sequence by direct sequencing using the forward and reverse primers. The nucleotide sequence has been deposited in the DDBJ/EMBL/GenBank databases under accession no. AB297681. Comparison

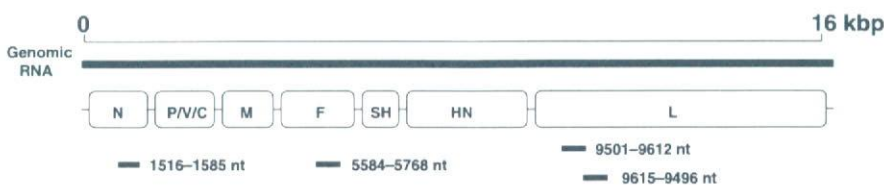


Fig. 1. Locations of PCR fragments of viral cDNAs amplified using the RDV method. The amplified PCR fragments were sequenced directly and mapped onto the avian paramyxovirus genome

of the nucleotide sequence of the L protein revealed that the isolate was closely related to APMV-6/duck/Taiwan/Y1/98, isolated in Taiwan in 1998, with 98.6% nucleotide identity.

RDV ver 2.0 is a rapid, sensitive method for the direct determination of avian viral RNA sequences in allantoic fluids inoculated with the test specimen. This method has the potential to become a standardized and qualified method for the detection of known and unknown avian RNA viruses.

Acknowledgments

We thank Dr. Y Sakoda (Hokkaido University, Sapporo, Japan) for useful suggestions and Ms. M. Ogata (National Institute of Infectious Diseases) for assistance. This work was supported in part by the Japan Health Science Foun-

dation, Tokyo, Japan. K.S. is a recipient of the Research Resident Fellowships from the Japan Health Science Foundation, Japan.

References

1. Chang PC, Hsieh ML, Shien JH, Graham DA, Lee MS, Shieh HK (2001) Complete nucleotide sequence of avian paramyxovirus type 6 isolated from ducks. *J Gen Virol* 82: 2157–2168
2. Endoh D, Mizutani T, Kirisawa R, Maki Y, Saito H, Kon Y, Morikawa S, Hayashi M (2005) Species-independent detection of RNA virus by representational difference analysis using non-ribosomal hexanucleotides for reverse transcription. *Nucleic Acids Res* 33: e65
3. Mizutani T, Endoh D, Okamoto M, Shirato K, Shimizu H, Arita M, Fukushi S, Saijo M, Sakai K, Lim CK, Nerome R, Takasaki T, Suzuki T, Kurane I, Morikawa S, Nishimura H (2007) Rapid genome sequencing of RNA viruses. *Emerg Infect Dis* 13: 322–324

Development of Recombinant Nucleoprotein-Based Diagnostic Systems for Lassa Fever[▽]

Masayuki Saijo,^{1*†} Marie-Claude Georges-Courbot,² Philippe Marianneau,² Victor Romanowski,³ Shuetsu Fukushi,¹ Tetsuya Mizutani,¹ Alain-Jean Georges,⁴ Takeshi Kurata,⁵ Ichiro Kurane,¹ and Shigeru Morikawa^{1†}

Department of Virology 1, National Institute of Infectious Diseases, 4-7-1 Gakuen, Musashimurayama, Tokyo 208-0011, Japan¹; Unit of Biology of Viral Emerging Infections, Institute Pasteur, IFR 128 Biosciences Lyon-Gerland, 21 Avenue Tony Garnier, 69365 Lyon Cedex 07, France²; Instituto de Bioquímica y Biología Molecular, Facultad de Ciencias Exactas, Universidad Nacional de a Plata, 1900 La Plata, Argentina³; Laboratory P4 Jean-Merieux-INSERM, 21 Avenue Tony Garnier 69365 Lyon Cedex 07, France⁴; and Department of Pathology, National Institute of Infectious Diseases, 1-23-1 Toyama, Shinjuku-ku, Tokyo 162-864, Japan⁵

Received 1 March 2007/Returned for modification 22 April 2007/Accepted 20 June 2007

Diagnostic systems for Lassa fever (LF), a viral hemorrhagic fever caused by Lassa virus (LASV), such as enzyme immunoassays for the detection of LASV antibodies and LASV antigens, were developed using the recombinant nucleoprotein (rNP) of LASV (LASV-rNP). The LASV-rNP was expressed in a recombinant baculovirus system. LASV-rNP was used as an antigen in the detection of LASV-antibodies and as an immunogen for the production of monoclonal antibodies. The LASV-rNP was also expressed in HeLa cells by transfection with the expression vector encoding cDNA of the LASV-NP gene. An immunoglobulin G enzyme-linked immunosorbent assay (ELISA) using LASV-rNP and an indirect immunofluorescence assay using LASV-rNP-expressing HeLa cells were confirmed to have high sensitivity and specificity in the detection of LASV-antibodies. A novel monoclonal antibody to LASV-rNP, monoclonal antibody 4A5, was established. A sandwich antigen capture (Ag-capture) ELISA using the monoclonal antibody and an anti-LASV-rNP rabbit serum as capture and detection antibodies, respectively, was then developed. Authentic LASV nucleoprotein in serum samples collected from hamsters experimentally infected with LASV was detected by the Ag-capture ELISA. The Ag-capture ELISA specifically detected LASV-rNP but not the rNPs of lymphocytic choriomeningitis virus or Junin virus. The sensitivity of the Ag-capture ELISA in detecting LASV antigens was comparable to that of reverse transcription-PCR in detecting LASV RNA. These LASV rNP-based diagnostics were confirmed to be useful in the diagnosis of LF even in institutes without a high containment laboratory, since the antigens can be prepared without manipulation of the infectious viruses.

Lassa fever (LF) is a viral hemorrhagic fever caused by Lassa virus (LASV), an Old World arenavirus. Many cases of LF occur in western Africa in countries such as Guinea, Sierra Leone, and Nigeria (7, 23, 27, 29–31). It is thought that LASV infects tens of thousands of humans annually and causes hundreds to thousands of deaths (34). Humans become infected through contact with infected excreta, tissue, or blood from the peridomestic rodent, *Mastomys natalensis*, the reservoir host of LASV (34). LASV can be transmitted to other humans via mucosal or cutaneous contact or through nosocomial contamination (27). More than 20 imported cases of LF have been reported outside the endemic region in areas such as the United States, Canada, Europe, and Japan (1, 2, 13, 15, 18, 24, 25). Recently, the potential for the use of hemorrhagic fever viruses, including LASV, as a biological weapon has been emphasized (5, 6). Therefore, the development of diagnostic systems for LF is important even in countries free from LF outbreaks to date.

Manipulation of infectious LASV is necessary for the detection of specific antibodies. However, a high-containment laboratory (biosafety level 4 [BSL-4]) is required for handling infectious LASV and, therefore, the preparation of LASV antigens cannot be implemented in institutes without a BSL-4 facility. Within this framework, it is important to develop sensitive and specific diagnostic systems for LF that eliminate the need for the manipulation of infectious LASV. In the present study, the recombinant nucleoprotein (rNP) of LASV (LASV-rNP) was expressed and evaluated for its ability to detect LASV antibodies. LASV-rNP-based enzyme-linked immunosorbent and indirect immunofluorescence assays (ELISA and IIFA) were developed. Furthermore, novel monoclonal antibodies to LASV-rNP were generated and used in combination with the recombinant antigen to develop an LASV antigen (nucleoprotein) capture ELISA. The present study presents an alternative strategy to develop diagnostic systems without handling infectious LASV.

MATERIALS AND METHODS

Cells. A HeLa cell line was cultured in the Eagle minimum essential medium supplemented with 10% fetal bovine serum and the antibiotics penicillin G and streptomycin (MEM-10FBS). Tn5 insect cells were used for the expression of the rNPs of arenaviruses (LASV, lymphocytic choriomeningitis virus [LCMV], and Junin virus [JUNV]) in a baculovirus system. The Tn5 insect cells were cultured as reported previously (38).

* Corresponding author. Mailing address: Special Pathogens Laboratory, Department of Virology 1, National Institute of Infectious Diseases, 4-7-1 Gakuen, Musashimurayama, Tokyo 208-0011, Japan. Phone: 81-42-561-0771, ext. 320. Fax: 81-42-561-2039. E-mail: msaijo@nih.go.jp.

† M.S. and S.M. contributed equally to this study.

▽ Published ahead of print on 18 July 2007.

Viruses. LASV (strain AV), which was isolated from an imported case of LF to Germany from West Africa, was used (13). The experimental process that required manipulation of infectious LASV was carried out in the BSL-4 laboratory in the P4 laboratory, INSERM, Lyon, France. Mopeia virus (MOPV), which belongs to the family *Arenaviridae*, genus *Arenavirus*, was also used. Recombinant NPs of LCMV (26) and JUNV (11), designated LCMV-rNP and JUNV-rNP, respectively, were also expressed in a baculovirus system and used in the study. A baculovirus (Ac- Δ P), which lacks polyhedrin expression, was used as a control virus (26). The virus titer of LASV in serum samples was determined by using a focus-forming unit (FFU) assay as described previously (3).

Sera. Four human serum samples—three samples serially collected from one patient with LF and one additional sample from another patient with LF—and ninety-six human sera collected from Japanese subjects with no history of travel to areas where LF is endemic were used as positive and negative controls, respectively. The patient with LF, from whom three serial serum samples were collected, was the first case of LF to be imported in Japan in 1987 (15). The other human serum sample was provided from the Special Pathogens Branch, National Center for Infectious Diseases, Centers for Disease Control and Prevention, Atlanta, GA.

Serum samples collected from five monkeys (*Macaca fascicularis*) subcutaneously infected with LASV strain AV at 10^1 FFU (two monkeys) or 10^7 FFU (three monkeys) and those collected from four monkeys with mock infection were also used. The serum samples used in the study were collected at 4 to 5 weeks postchallenge.

Five hamsters were subcutaneously infected with 10^5 FFU of LASV, strain AV, and blood was drawn on days 0, 4, 11, and 16 postinfection, taking the day on which the virus was inoculated as day 0. Serum fractions of the collected blood specimens were separated and tested for LASV antigen by antigen capture (Ag-capture) ELISA and reverse transcription-PCR (RT-PCR).

Rabbit sera (polyclonal antibodies) were raised against LASV-rNP, LCMV-rNP, and JUNV-rNP by immunization of rabbits with the purified LASV-rNP, LCMV-rNP, and JUNV-rNP, respectively, in the form of a mixture with the adjuvant, Inject Alum (Pierce). Rabbits were immunized with sufficient amount of the purified nucleoproteins of each virus three times with an interval of 2 weeks. After confirmation of the increased titer, $>10,000$ times as determined by indirect immunofluorescence assay, which was developed in the present study, blood was drawn from the rabbits, and the serum fraction was used in the present study.

Recombinant baculovirus. In order to construct the transfer vector, a cDNA clone of NP from LASV strain Josiah was used. The cDNA was kindly provided by J. B. McCormick, former Director of the Special Pathogens Branch, National Centers for Infectious Diseases, Centers for Disease Control and Prevention. The complete nucleotide sequence of the NP gene is registered in GenBank under the accession number NC_004296. The DNA of the LASV-NP was amplified by PCR from the source using the primers LAS-NiB (5'-GTGGATCCAACACAACAATCTGG-3'; the BamHI restriction site is underlined) and LAS-NiB (5'-CCGGATCCCAITTTACAGAACGACTC-3'). The PCR conditions were the same as previously reported (38). The 1,743-bp amplification product was digested with BamHI and subcloned into the BamHI site of pQE32 vector DNA (QIAGEN GmbH, Hilden, Germany) to construct pQE32-LASV-NP. The inserted LASV-NP DNA was sequenced by using appropriate primers with an ABI Prism 310 genetic analyzer (PE Applied Biosystems, Foster City, CA) and confirmed to be in proper orientation downstream the promoter and identical to the original sequence. The DNA fragment of LASV-NP with a histidine (His) tag was isolated from the plasmid, pQE32-LASV-NP, by digestion with EcoRI and HindIII. It was then blunt repaired with Klenow enzyme and ligated into the blunt-ended BamHI site of pACYM1 (26). The resulting recombinant transfer vector with the correct orientation with respect to the polyhedrin promoter was constructed (pACYM1-His-LASV-NP). Tn5 insect cells were transfected with mixtures of purified *Autographa californica* nuclear polyhedrosis virus (AcMNPV) DNA and pACYM1-His-LASV-NP according to the procedures described by Kitts et al. (20), with the modification of Matsuura et al. (26). Recombinant baculovirus was then isolated. The baculovirus, which expressed His-tagged LASV-rNP (His-LASV-rNP), was designated Ac-His-LASV-NP.

The baculovirus, Ac-LCMV-NP, which expressed LCMV-rNP, was used in the study (26).

The recombinant baculovirus that expressed JUNV-rNP, Ac-JUNV-NP, was generated as follows. The gene encoding the NP of JUNV (strain MC2) was reconstructed from cloned cDNA. The nucleotide sequence of the interest gene was deposited in GenBank under accession number D10072 (12). A complete NP gene with the initiation and stop codons amplified by PCR using appropriate primers, which possessed BamHI restriction sites. The entire DNA product of JUNV-NP was digested with BamHI and ligated into the transfer vector

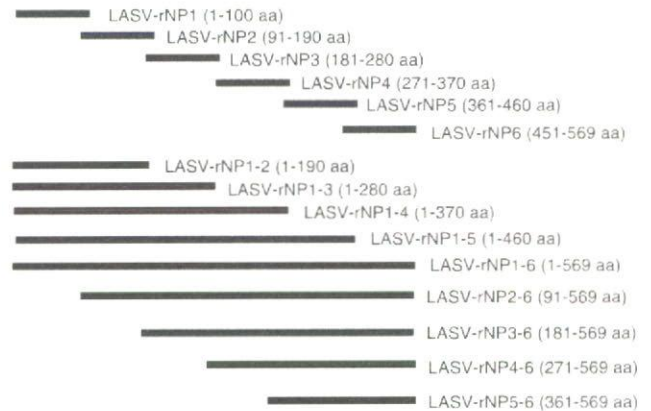


FIG. 1. Schematic representation of truncated LASV-rNP expressed as a form of GST fusion protein in *E. coli* transformed with the corresponding expression vector. The description "LASV-NP1-6" in the middle portion of the figure indicates full-length LASV-rNP.

pAcUW2B (28). Clones containing the insert in the correct orientation were selected, and the plasmid DNA was used for cotransfection in Sf21 cells with a polyhedrin-positive AcMNPV DNA, and the supernatant culture was screened for a polyhedrin-negative phenotype by plaque assay (19). Finally, recombinant baculovirus clones overexpressing JUNV-rNP were obtained after three successive plaque purifications. One of them, designated AcMNPV-Jun-N122, was used in the present study and is referred to hereafter as Ac-JUNV-NP.

Expression and purification of His-LASV-rNP, LCMV-rNP, and JUNV-rNP. Tn5 cells infected with Ac-His-LASV-NP were incubated at 26°C for 72 h. The cells were then washed twice with cold phosphate-buffered saline (PBS) solution. A preliminary study demonstrated that most of the Tn5 cellular proteins were solubilized in PBS containing 2 M urea (PBS-2 M urea) but that the His-LASV-rNP was insoluble and that the LASV-rNP could be solubilized in PBS containing 8 M urea (PBS-8 M urea). Therefore, the Tn5 cells infected with Ac-His-LASV-NP were first suspended in PBS-2 M urea. After the centrifugation of the cell suspensions at $15,000 \times g$ for 10 min, the pellet fractions were collected and then were solubilized in PBS-8 M urea. After the centrifugation of the samples, the supernatant fractions were used as the purified antigens. LCMV-rNP and JUNV-rNP showed dissolution characteristics in urea similar to those of His-LASV-rNP; therefore, LCMV-rNP and JUNV-rNP were also fractionated in the same way as the His-LASV-rNP. The control antigen was produced from Tn5 cells infected with Ac- Δ P in the same manner as that for the positive antigens. The His-LASV-rNP was also purified by using the Ni²⁺ column purification method as reported previously (38). The source for His-LASV-rNP-purification was the supernatant fraction of the PBS-8 M urea-treated Tn5 cells infected with Ac-His-LASV-NP after sufficient dilution with PBS in order to reduce the urea concentration.

SDS-PAGE. The expression and purification efficiency of His-LASV-rNP, LCMV-rNP, and JUNV-rNP were analyzed on sodium dodecyl sulfate-polyacrylamide gel electrophoresis (SDS-PAGE) gels (12% polyacrylamide) after staining with Coomassie blue.

Establishment of MAbs. Monoclonal antibodies (MAbs) were generated as previously described (32, 41). BALB/c mice were immunized with purified His-LASV-rNP in the present study. Isotypes of the MAbs were determined by using a mouse MAb isotyping kit (Life Technologies).

Expression of truncated NPs of LASV. In order to determine the epitope of the MAbs to the His-LASV-rNP, truncated LASV-rNPs were expressed as a form of fusion protein with glutathione *S*-transferase (GST) as shown in Fig. 1. The DNA corresponding to each of the truncated NP fragments was amplified with the designed primers. The amplified DNA was subcloned into the BamHI and EcoRI cloning sites of plasmid pGEX-2T (Amersham Pharmacia Biotech, Buckinghamshire, England). Each insert was sequenced and confirmed to be in the correct frame and identical to the original sequence. The GST-tagged nucleoprotein fragments were expressed in an *Escherichia coli* BL21 system.

Western blotting. The MAbs were tested for reactivity to His-LASV-rNP and its fragments by Western blotting as reported previously (17, 32, 41).

Peptscan analyses. ELISA was performed as reported previously with the purified rNP or partial nucleoprotein peptides as the antigen (33). The peptides

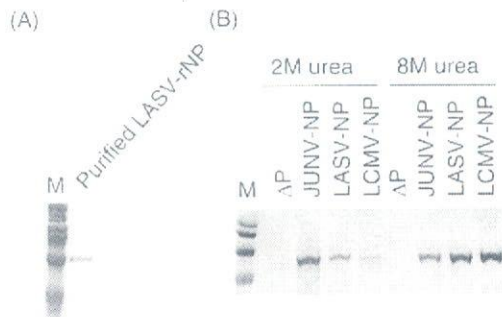


FIG. 2. SDS-PAGE analyses of the purification of His-LASV-rNP using the Ni^{2+} column purification method (A) and of the semipurification strategy based on the hydrophobic property of arenavirus nucleoproteins (B). The supernatant fractions of the Ac- ΔP -, Ac-His-LASV-NP-, Ac-LCMV-NP-, or Ac-JUNV-NP-infected Tn5 cells treated with PBS-2 M urea (B, left part) are shown. The pellet fractions of these cells treated with PBS-2 M urea were further solubilized with PBS-8 M urea (B, right part).

were shifted by 1 amino acid (aa), with a consecutive overlap of 9 aa to cover the entire LASV-NP1 (aa 1 to 100) and LASV-NP5 (aa 361 to 460) fragments. Linear epitopes on the NP were determined by using Pepsan (Chiron Technologies, Clayton, Australia) according to the manufacturer's instructions. Ninety-six peptides were prepared as 14-aa biotinylated peptides, including a 4-aa spacer sequence (SGSG) at the amino-terminal end, according to each of the amino acid sequences of the LASV-rNP1 and LASV-rNP5 of the LASV Josiah strain. The methods were previously described in detail (33).

IgG-ELISA. Immunoglobulin G (IgG)-ELISA was performed as previously described except for the antigen preparation (38, 39). Briefly, ELISA plates (96-well type plate, Pro-Bind; Falcon; Becton Dickinson Labware, Franklin Lakes, NJ) were coated with the predetermined optimal quantity of purified His-LASV-rNP, LCMV-rNP, or JUNV-rNP (approximately 100 ng/well) at 4°C overnight. Then, each well of the plates was inoculated with 200 μl of PBS containing 5% skim milk and 0.05% Tween 20 (M-T-PBS), followed by incubation for 1 h for blocking. The plates were washed three times with T-PBS and then inoculated with the test samples (100 μl /well), which were diluted fourfold from 1:100 to 1:6,400 with M-T-PBS. After a 1-h incubation period, the plates were washed three times with T-PBS, and then the plates were inoculated with goat anti-human IgG antibody labeled with HRPO (1:1,000 dilution; Zymed Laboratory). After a further 1-h incubation period, the plates were washed and 100 μl of ABTS [2,2'-azino-bis(3-ethylbenzothiazolinesulfonic acid)] solution (Roche Diagnostics, Mannheim, Germany) was added to each well. The plates were incubated for 30 min at room temperature, and optical density at 405 nm (OD_{405}) was measured against a reference of 490 nm. The adjusted OD_{405} was calculated by subtracting the OD of the negative antigen-coated wells from that of the corresponding wells. The means and standard deviations were calculated from the 96 control sera. The cutoff value for the assay was defined as the mean plus 3 standard deviations.

Immunofluorescence. The pQE32-LASV-NP was digested with BamHI, and the insert was subcloned into the BamHI site of the pKS336 vector (40). The LASV-NP gene that was inserted into the pKS336 vector, pKS336-LASV-NP, was confirmed to be in the correct orientation to the promoter, tested for nucleotide sequencing as described above, and the nucleotide sequence of the gene was confirmed to be identical to the original sequence. HeLa cells were then transfected with pKS336-LASV-NP by using a FuGENE6 transfection reagent (Roche Diagnostics) according to the manufacturer's instructions. The cells transfected with the plasmid were selected with 3 μg of blasticidin *S*-hydrochloride/ml in MEM-10FBS. The HeLa cell clones were analyzed for the expression of LASV-rNP by IIFA using the rabbit serum raised against His-LASV-rNP. The cells expressing LASV-rNP were subcloned and used as IIFA antigens.

Ag-capture ELISA. Ag-capture ELISA was performed as previously described (32, 41). The purified MAb to His-LASV-rNP, MAb 4A5, produced in the present study was diluted in PBS solution, and 100 μl was adsorbed overnight at 4°C onto the immunoplates (96-well type plate, Pro-Bind; Falcon; Becton Dickinson Labware). Purified MAb 4A5 was coated onto the immunoplates at a concentration of approximately 100 ng/well in 100 μl of PBS. The difference in the procedures between the Ag-capture ELISA in the present study and those in

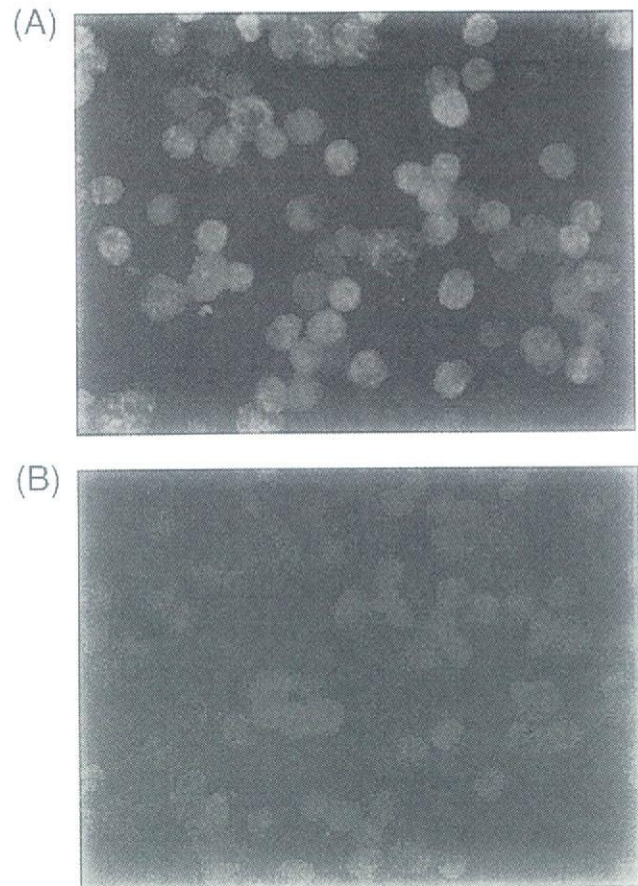


FIG. 3. Staining patterns of LASV-rNP-expressing HeLa cells by sera from an LF patient (A) and a healthy control (B) in an IIFA.

previous studies (32, 37, 41) is that the MAb, MAb 4A5, and rabbit serum raised to His-LASV-rNP were used as capture and detector antibodies, respectively. The procedure for the Ag-capture ELISA was performed as follows. The ELISA plate was coated with capture MAb, followed by blocking of the plate with M-T-PBS, addition of the samples to the ELISA plate, detection of the captured LASV-NP with rabbit serum raised to His-LASV-rNP, detection of rabbit IgG antibody that reacted with the captured antigen with goat anti-rabbit IgG antibodies conjugated with HRPO (Zymed Laboratories), and substrate reaction. In each run of the Ag-capture ELISA, the negative control antigen (M-T-PBS) was also tested. Serially diluted samples were added to the MAb-coated wells. The OD_{405} values of each well were adjusted by subtracting the OD_{405} value of the negative control antigen from the corresponding well. The adjusted OD_{405} was taken as a measure of the amount of antigen specifically bound. All samples were treated with 1% Nonidet-P40 (NP-40) in PBS to destroy the LASV virion and expose the nucleoprotein in the LASV virion.

RT-PCR. RT-PCR was performed as previously described (10). The primers used in the RT-PCR were 36E2 (5'-ACCGGGGATCCTAGGCATT-3') and 80F2 (5'-ATATAATGATGACTGTTGTTCTTTGTGCA-3'). The RT-PCR was carried out with a Ready-to-Go RT-PCR tube (Pharmacia). The amplified PCR products were visualized with ethidium bromide in 2% agarose gel after electrophoresis.

RESULTS

Expression of His-LASV-rNP. Tn5 cells infected with each of the recombinant baculoviruses—Ac-His-LASV-NP, Ac-LCMV-rNP, and Ac-JUNV-rNP—were suspended in PBS-2 M urea. Most of the cell proteins were solubilized by this